NASA Contractor Report 187557

Fuselage Shell and Cavity Response Measurements on a DC-9 Test Section

M.A. Simpson, G.P. Mathur,
M.R. Cannon, B.N. Tran, and P.L. Burgé

DOUGLAS AIRCRAFT COMPANY
MCDONNELL DOUGLAS CORPORATION
LONG BEACH, CA 90846

CONTRACT NAS1-18037
AUGUST 1991

National Aeronautics and
Space Administration

Langley Research Center
Hampton, Virginia 23665-5225

NASA Contractor Report 187557

Fuselage Shell and Cavity Response Measurements on a DC-9 Test Section

M.A. Simpson, G.P. Mathur,
M.R. Cannon, B.N. Tran, and P.L. Burgé

DOUGLAS AIRCRAFT COMPANY
MCDONNELL DOUGLAS CORPORATION
LONG BEACH, CA 90846

CONTRACT NAS1-18037
AUGUST 1991

National Aeronautics and
Space Administration

Langley Research Center
Hampton, Virginia 23665-5225

Preface

This report was prepared by McDonnell Douglas Corporation under Task Assignment 8, Subtask 1 of Contract NAS1-18037 with NASA Langley Research Center. The NASA technical monitor was Dr. Kevin P. Shepherd.

Several individuals at Douglas Aircraft Company made major contributions to this study. The various tests described in this report were conducted by Don Daulton, Jim Phillips, and Dick Gordon, under the direction of Dr. Mark Lang. Mike Sundquist and Brian Hoare were responsible for data processing. Dr. Mahendra Joshi reviewed the report and offered many constructive comments.

Contents

List of Figures

1 Introduction

This report documents the results of a series of fuselage shell and cavity response measurements which were conducted in the Fuselage Acoustics Research Facility (FARF) at Douglas Aircraft Company with a DC-9 aircraft aft section as the test fuselage. The specific objectives of the measurements were to:

- Define the shell and cavity modal characteristics of the test fuselage
- Understand the structural-acoustic coupling characteristics of the test fuselage
- Measure the response of the test fuselage to different types of acoustic and vibration excitation

To accomplish these objectives, the fuselage structure and the cabin cavity were excited with either a single acoustic source inside the cabin, a single acoustic source outside the fuselage, an array of acoustic sources outside the fuselage, a point mechanical source attached to the fuselage shell, or a combination of the mechanical source and the single exterior acoustic source. The response of the fuselage shell to these inputs was measured with an array of accelerometers attached to the fuselage skin, and the response of the cabin cavity was measured with an array of microphones located inside the cabin. From these measurements, spatial plots of the shell acceleration and cabin acoustic pressure field were produced. In addition, wavenumber-frequency analysis techniques were applied to the test data to generate acceleration and pressure wavenumber maps corresponding to the spatial plots. Analysis and interpretation of these spatial plots and wavenumber maps provided the required information on modal characteristics, structural-acoustic coupling, and fuselage response, and also demonstrated the usefulness of wavenumber analysis techniques in understanding fuselage structural-acoustic behavior.

The next section of this report describes the test program. Detailed test results are provided in Sections 3 through 5. Section 3 presents the measured shell and cavity modal characteristics. In Section 4 the coupling characteristics of the fuselage structure and cabin cavity are discussed. Section 5 describes the response of the fuselage to the different excitations used in the test program. Major conclusions are summarized in the final section.

2 Description of the Test Program

The tests were conducted between October 1989 and January 1990 in the Fuselage Acoustics Research Facility (FARF) at Douglas Aircraft Company (DAC). This facility consists of the aft section of a DC-9 aircraft fuselage, noise and vibration sources to simulate a variety of excitations including advanced turboprop excitation, a multi-channel digital data acquisition and processing system, and an anechoic chamber to house the fuselage section. Figure 1 shows the fuselage test section, with the frame station and longeron numbering system. Additional details about FARF and its components may be found in Reference [1].

2.1 Fuselage Configuration

The DC-9 aft fuselage section was configured to be similar to the Baseline Configuration of the MD-UHB Demonstrator. On the Demonstrator, several treatments were installed which were designed to reduce cabin noise levels arising from the acoustic and mechanical loads generated by the UHB engine. The specific treatments installed for the Baseline Configuration consisted of additional frames in the aft cabin (including a torque box frame), damping material on the new and existing frames, a double wall attached to the pressure bulkhead, sonic fatigue damping material applied to the skin in the aft section and cabin area, acoustic damping material applied to the skin in the cabin and cargo compartments, floor isolation, and absorption blankets in the aft section. The cabin was unfurnished, but included two layers of sidewall thermal insulation. Reference [2] provides a complete description of each treatment and fuselage configuration incorporated in the Demonstrator flight test program.

For the current ground tests in FARF, the same treatments were installed in the DC-9 fuselage section, except for the aft bulkhead double wall and the aft section absorption blankets. These two treatments were considered unnecessary for these tests since the acoustic and vibration sources were not located at the aft of the aircraft (in contrast to the aft-mounted engines on the Demonstrator), and thus there was no energy contribution from the propagation path through the aft section. Other differences between the FARF fuselage and the Demonstrator were (1) no lavatories in FARF (they were previously removed and covered over with hard walls); (2) no floor isolation in FARF; and (3) uniform application of damping material around the entire FARF fuselage circumference (on the Demonstrator the sonic fatigue damping material is installed only on the UHB engine side).

To simulate in-flight conditions, the fuselage was pressurized to a pressure differential of 5 psi during all tests.

2.2 Noise and Vibration Sources

The fuselage shell and cavity were excited by six types of noise and/or vibration sources (four acoustic, one mechanical, and one a combination of acoustic and mechanical). The excitations were:

1. Broadband acoustic excitation of the interior cabin by a single loudspeaker.
2. Broadband mechanical (vibration) excitation of the fuselage structure by a single shaker.
3. Broadband acoustic excitation of the exterior of the structure by a single loudspeaker.
4. Acoustic excitation of the exterior of the structure by a single loudspeaker with 8 sine tones.
5. Acoustic excitation of the exterior of the structure by an array of 5 loudspeakers with 8 sine tones, and with time delays between each speaker to simulate the wave-trace velocity effects of a rotating propeller.
6. Broadband mechanical and acoustic excitation of the structure (achieved by combining excitations 2 and 3 above).

Figure 2 shows the single interior loudspeaker, located at the forward right corner of the cabin at station 480 and pointed at 45 degrees towards the cabin centerline. The exterior sources are depicted in Figure 3; Figure 1 shows their longitudinal locations relative to the fuselage. The single shaker is mounted on a support structure, and attached to the right side of the fuselage at station 718, longeron 9. The exterior array of five loudspeakers is located on a support stand on the left side of the fuselage at station 661. The center speaker of this vertical, linear array was used for single speaker acoustic excitation. Figures 4 and 5 are photographs of the loudspeaker and shaker sources, respectively. All acoustic sources are Altec 15-inch drivers mounted in JBL ported speaker enclosures. The vibration source is a VTS-100 electrodynamic shaker.

For the broadband excitations, a Hewlett-Packard 8057A noise generator was used to produce pink noise, which was subsequently filtered to provide a signal between about 100 and 1000 Hz, amplified, and fed to the interior or exterior loudspeaker or shaker as required. The excitation levels were as follows: from the interior loudspeaker, approximately 100 dB in each one-third octave band between 100 and 1000 Hz, measured by the interior reference microphone 39 inches in front of the speaker; from the exterior loudspeaker, approximately 113 dB in each one-third octave band between 100 and 1000 Hz, measured by the exterior reference microphone on the surface of the fuselage three feet from the loudspeaker; from the shaker, 30 lbs force measured by the force gauge between the shaker and the fuselage.

For the sine tone excitations, the following eight tones, generated by separate Dynatech 200MSTPC function generators, were used simultaneously: 100, 125, 160, 168, 200, 210, 250, and 315 Hz. The 168 and 210 Hz tones represent the blade passage frequencies of the aft and forward rotors of a UHB engine with 10x8 rotor configuration, while the remaining six tones represent the center frequencies of the one-third octave bands from about 90 to about 350 Hz, the primary frequency range of interest for UHB aircraft. For the single loudspeaker tests, the excitation levels were approximately 110 dB for each tone, measured by the exterior reference microphone.

The acoustic excitation involving all five loudspeakers and all eight tones was designed to simulate the wave-trace velocity effects associated with rotating propeller sources. To accomplish this, a special support stand was built to accommodate the five speakers along an arc with radius corresponding to the UHB propeller radius (approximately 11 feet). In addition, a time delay of 4 msec was set up between the signals through each of the speakers, starting with the lowest speaker (to simulate propeller upsweep effects). This delay corresponds to a propeller rotational speed of about 1260 rpm, which is typical of the rotational speeds used during the Demonstrator flight tests. The excitation levels were between 107 and 115 dB for each tone, measured by the exterior reference microphone.

2.3 Measurement and Processing Instrumentation

Four types of data were measured during the test program: exterior noise levels during exterior acoustic excitation; fuselage acceleration levels during all excitations except interior acoustic excitation; interior noise levels during all excitations; and force levels during mechanical excitation. The number, spacing, and placement of transducers on the fuselage surface and within the cabin were selected to provide measurement data over sufficiently large regions for subsequent acceleration and pressure spatial plots, and to ensure sufficient resolution in the circumferential and longitudinal (or axial) directions for subsequent acceleration and pressure wavenumber maps.

Exterior microphones were mounted on the left side of the fuselage 1/2 inch from the fuselage surface in a row longitudinally along longeron 15, and circumferentially along station 661 (see Figure 6). The microphone at the intersection of longeron 15 and station 661, opposite the center of the exterior loudspeaker array, was used as a reference for the exterior measurements. Each exterior microphone measurement system consisted of a B&K 4134 1/2 inch microphone with a Genrad 1560-P42 preamplifier and Pacific and Ithaco amplifiers.

An array of accelerometers was also mounted on the left side of the fuselage (Figure 6). This 13x15 array had a longitudinal spacing of 9.5 inches and a circumferential

spacing of 15.4 inches. In addition to this array, accelerometers were mounted in a row longitudinally just under longeron 9, and on the right side of the fuselage circumferentially at stations 661 and 718 (which, in conjunction with the accelerometers on the left side at these two stations, formed two accelerometer rings around the entire fuselage). The accelerometer on the left side at station 718 just under longeron 9 was used as a reference accelerometer for the vibration measurements. Each accelerometer measurement system consisted of an Endevco 2250A-10 accelerometer with an Endevco signal conditioner and Ithaco amplifier.

Within the cabin, the array of 75 microphones shown in Figure 7 was used to measure interior noise levels at 13 stations (approximately 19 inches apart) from station 547 to station 779. For these measurements the reference microphone was located on the cabin centerline, approximately 20 inches above the floor and 40 inches in front of the interior loudspeaker at the front of the cabin. The interior microphone measurement system was identical to the exterior microphone system.

A force gauge was installed between the connecting rod (stinger) of the shaker and the fuselage. This transducer was used as a reference for the shaker input to the structure. The force measurement system consisted of a B&K 8500 force gauge with B&K 1050 vibration exciter and Ithaco amplifier.

The number of unique transducer locations included 16 exterior microphone locations, 234 accelerometer locations, 976 interior microphone locations, and 1 force gauge location. A total of over 7100 test points was collected during the entire test program. In order to collect this amount of data, transducer signals were recorded in sets on FM tape, at up to 26 channels simultaneously. Each measurement sample included a recording of the appropriate reference transducer so that data collected at different times could be normalized to a common excitation.

The microphone channels were calibrated periodically with a B&K 4220 pistonphone, which produces a constant 250 Hz signal at 124 dB. The accelerometer channels were similarly calibrated with a B&K 4294 calibrator exciter which produces a constant 159 Hz signal at 1 g (rms). The various amplifiers were set to provide a 1 volt input to the tape recorder corresponding to either 124 dB or 1 g, depending on transducer type. This same 1 volt signal level was then used as a surrogate calibration signal on subsequent data tapes.

Measured data were recorded on a Honeywell model 101 FM tape recorder. Annotation information and a time code were recorded on two additional recorder channels. The data tapes were then processed on a custom-designed digital data acquisition and processing system (DDAPS). DDAPS consists of a special digitizer coupled to a DEC microVAX II computer, and is designed to permit rapid calculation and display of a variety of time-series functions from which frequency domain data can subsequently

be obtained. The system is capable of simultaneous sampling of up to 32 channels of analog data at a rate of 12,600 samples/second/channel for up to 2 minutes, covering a frequency range of up to 4 kHz. The sampling duration for each measurement in this test program was 1 minute, which was sufficient to provide the frequency resolution (0.78 Hz) used in the subsequent analyses.

DAC in-house software operating on a DEC VAX 8300 coupled with a Numerix MARS 432 array processor was used to convert the digitized time series data into auto- and cross-spectra for the various measurement locations, with respect to the appropriate reference transducer. These spectra were further processed to meet the requirements of subsequent analyses or to provide graphic output for presentation purposes. In addition, for the wavenumber-frequency analyses, DAC in-house software was used to obtain wavenumber maps by implementing a two-dimensional Fourier transform on the spatial domain data.

Although the test signals were generated over a frequency range from about 100 to 1000 Hz for the broadband excitations, for the test results reported here the data analyses were limited to frequencies below 500 Hz.

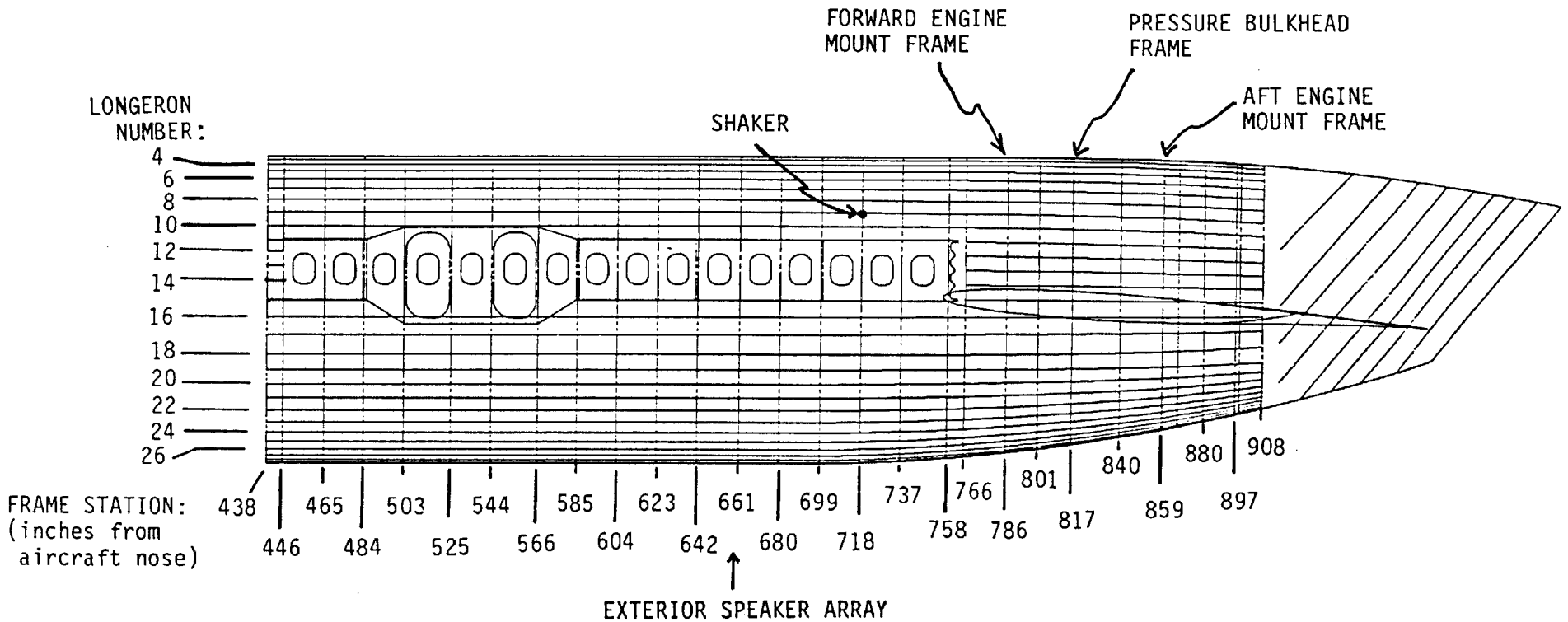

Figure 1. The DC-9 Fuselage Test Section, Showing Frame and Longeron Numbering

Figure 2. Photograph of the Fuselage Interior in the Baseline Configuration, Showing the Interior Loudspeaker

ORIGINAL PAGE
BLACK AND WHITE PHOTOGRAPH

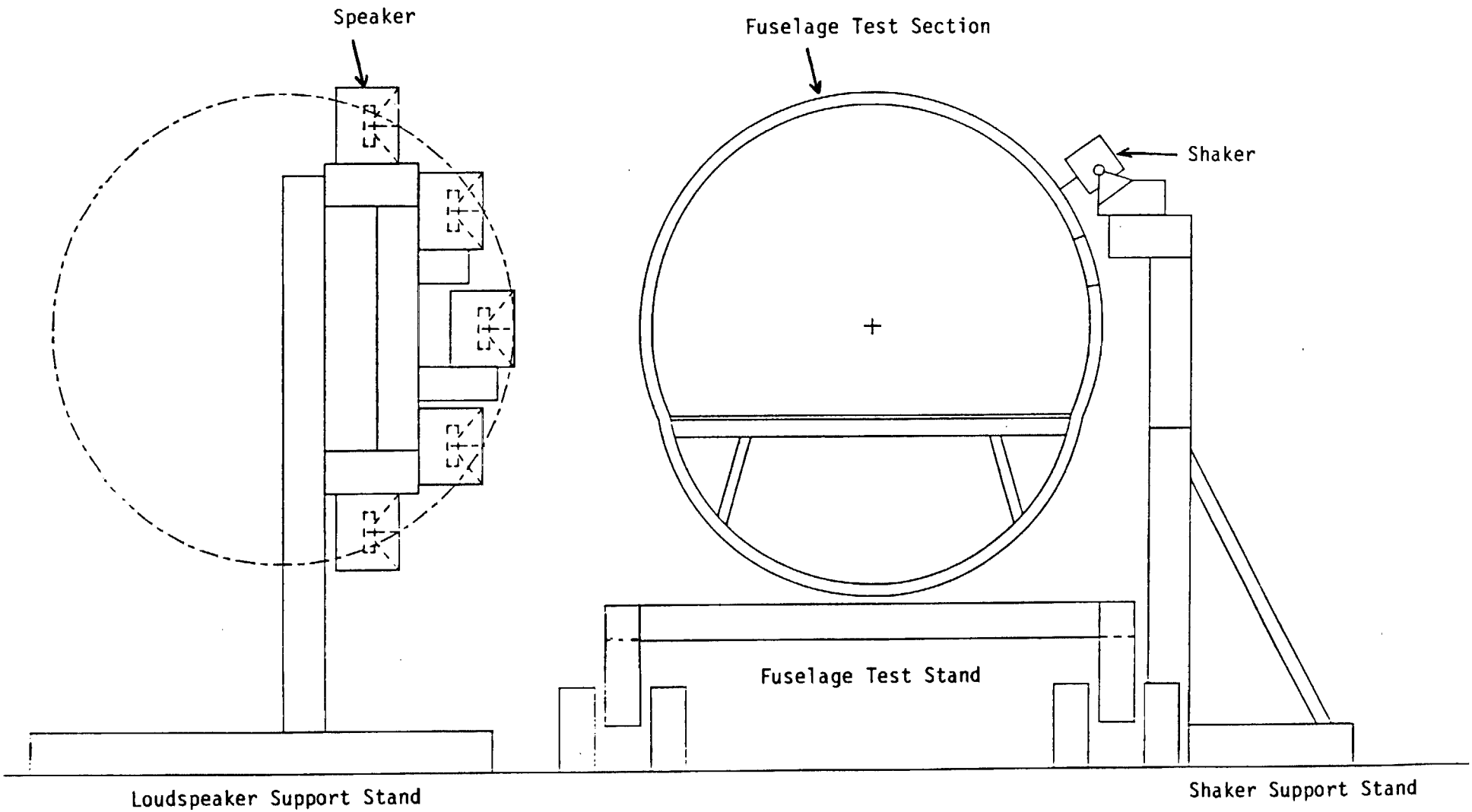

Figure 3. The Location of the Loudspeaker and Shaker Exterior Sources

Figure 4 Photograph of the Exterior Loudspeakers and the Left Side of the Fuselage

ORIGINAL PAGE
BLACK AND WHITE PHOTOGRAPH

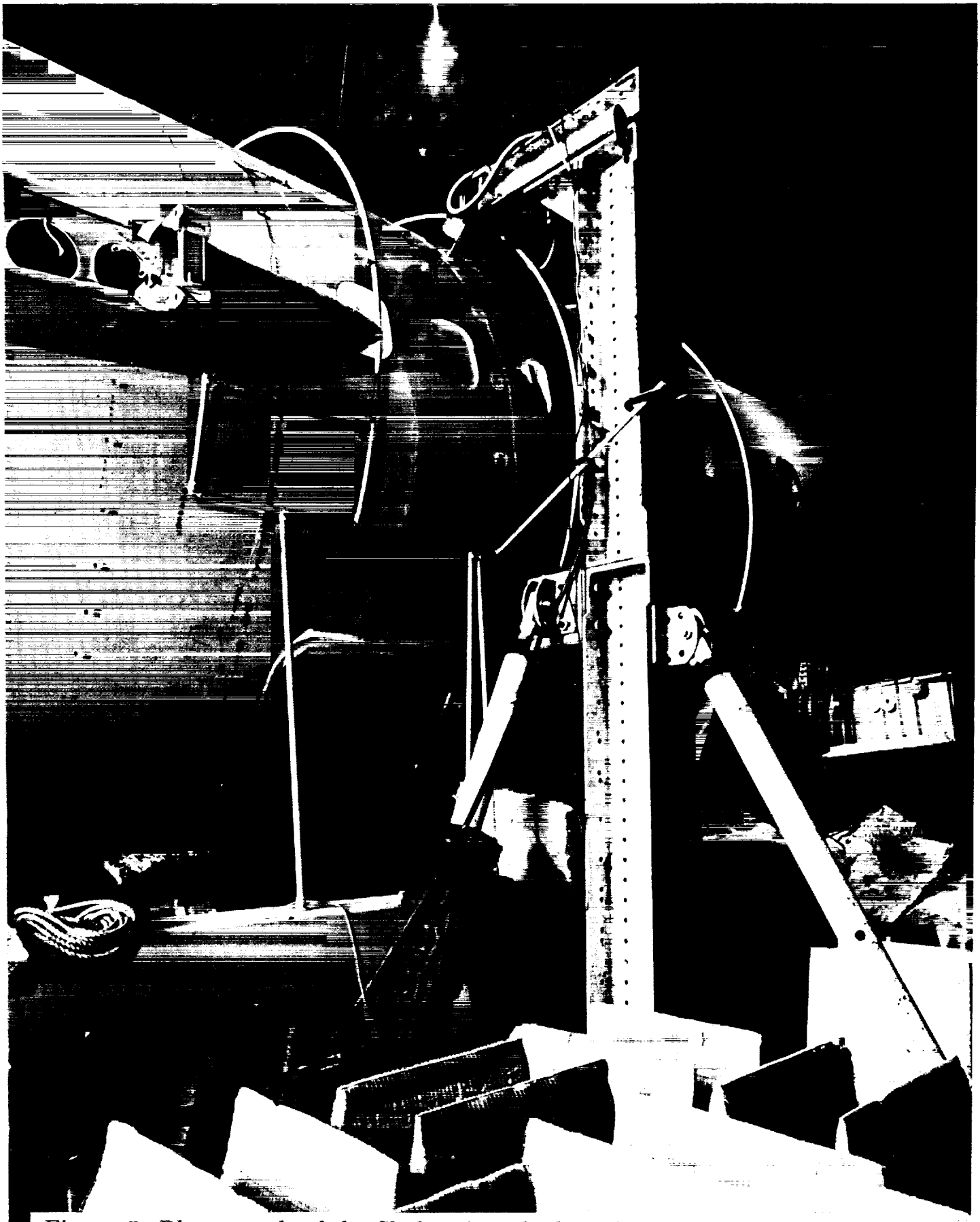

Figure 5. Photograph of the Shaker Attached to the Right Side of the Fuselage

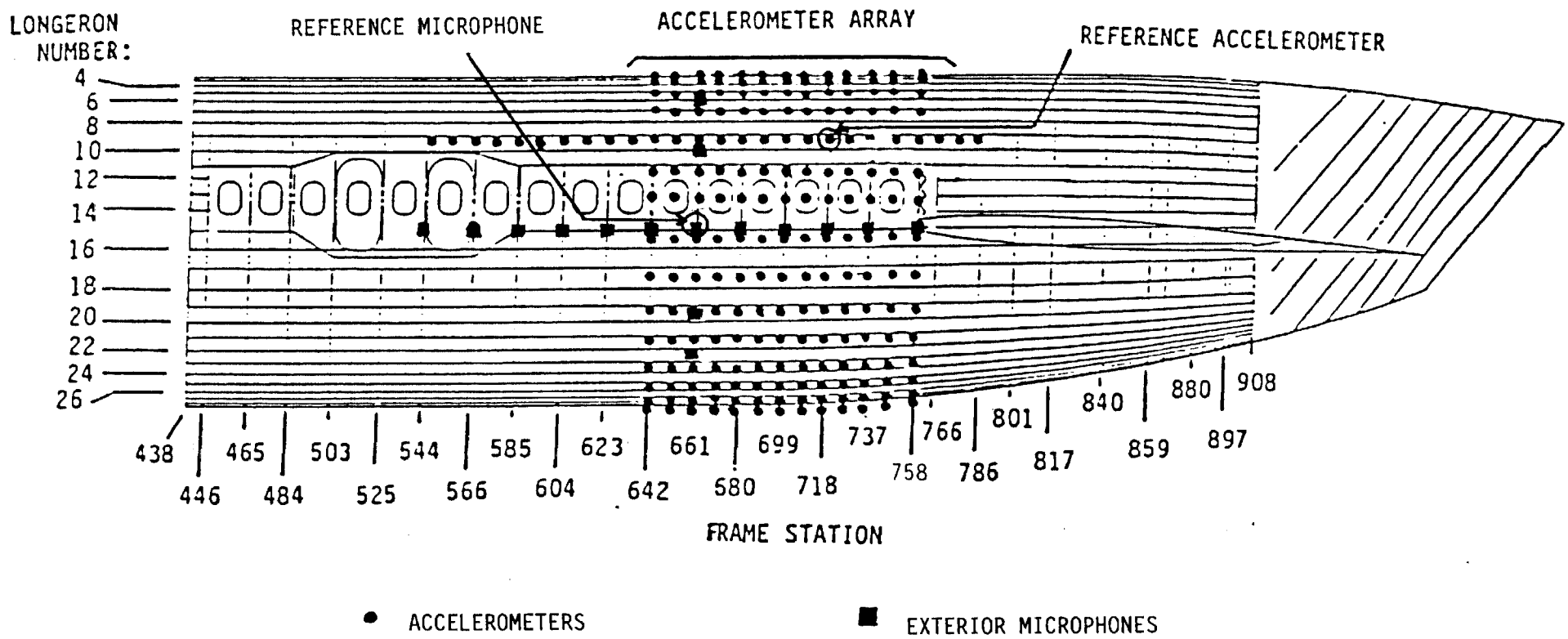

Figure 6. Location of the Exterior Microphones and Accelerometers

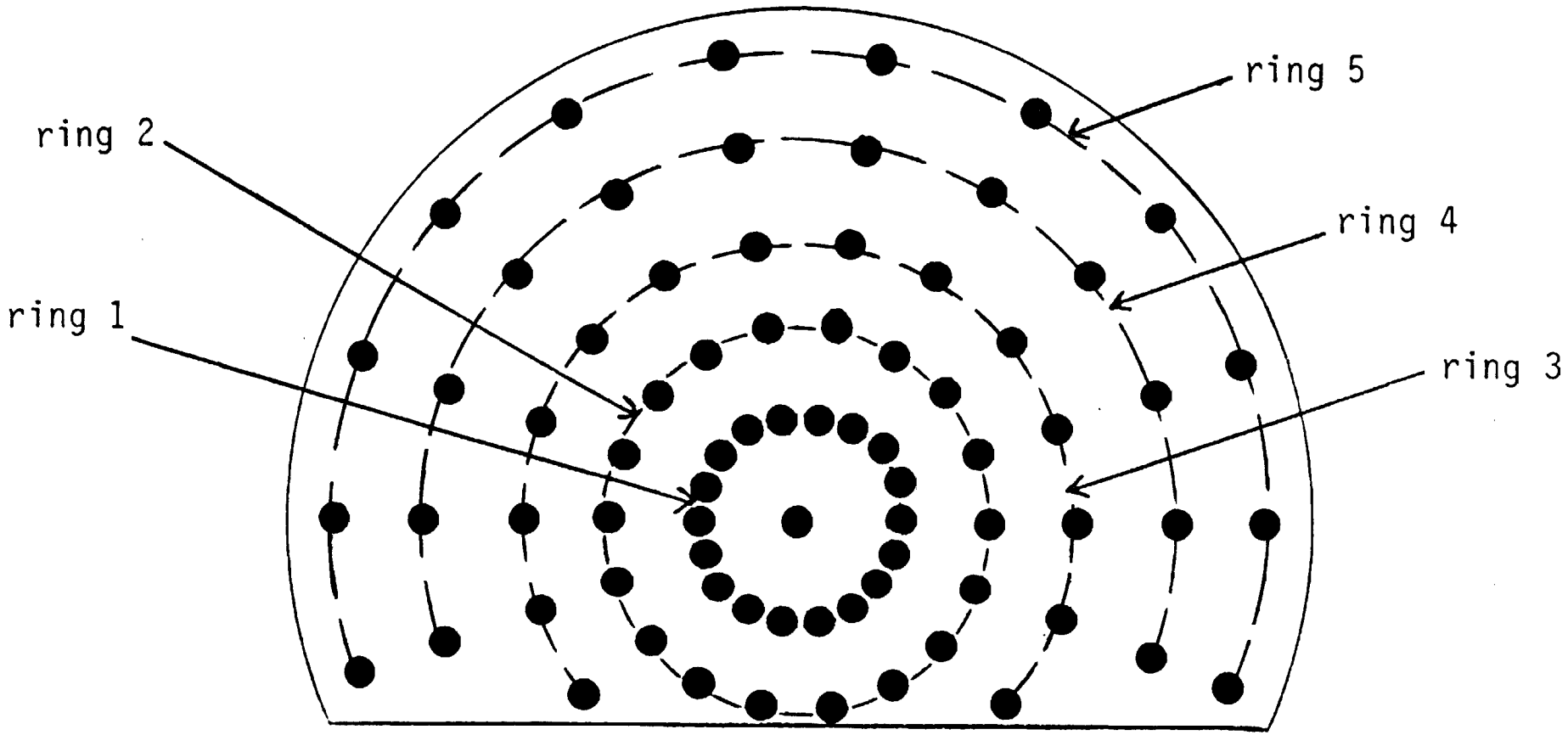

Figure 7. The Interior Microphone Array

3 Fuselage Modal Characteristics

Measured fuselage acceleration levels and cabin noise levels under selected excitations were used to define the structural and cavity modal characteristics of the fuselage. Specifically, the frame structural modes and uncoupled and coupled cavity modes at station 718 were studied. To determine the structural modes and coupled cavity modes, shaker broadband mechanical excitation was used. To determine the uncoupled cavity modes, interior loudspeaker broadband excitation was used.

3.1 Frame Structural Modes

To define the structural modes for frame 718, transfer functions between the input force (applied to the right side of the fuselage at frame 718, longeron 9) and the response acceleration were computed from the measured data for each of the 28 accelerometers on this frame. Figure 8 shows a sample transfer function spectrum for the accelerometer on the left side of the fuselage at longeron 9 between 90 and 200 Hz. Peaks in the transfer function spectra indicate those frequencies at which modes may occur. Based on these spectral peak frequencies for all the transfer functions, the following were judged to be the modal frequencies for frame 718 (in Hz):

95	176	314
105	187	366
108	200	380
112	221	394
118	232	420
130	256	440
134	266	450
146	274	480
151	292	
165	304	

For each frequency, the frame mode shape (or structural deformation) was determined by plotting the displacement measured at each accelerometer. Sample frame modes determined in this manner are shown Figure 9, for 95 and 108 Hz. In this figure the solid line represents the undeformed frame ring while the dashed line represents the measured frame deformation. The frame is viewed facing aft, so that the excitation point is at the upper left side of the ring.

3.2 Cabin Cavity Modes

To define the frequencies of the transverse (across-the-cabin) cavity modes at station 718, transfer functions between the input signal at the appropriate reference transducer and the response acoustic pressure were computed from the measured data at each of the 75 response microphones in the measurement array across the cabin at this station. The real and imaginary parts of these transfer functions were separately added together for all the response microphones. Plots of these summed real and imaginary values were examined to find the frequencies at which the real value was zero (or near zero) and the imaginary value was at (or near) a peak in the spectrum. Figure 10 shows how this approach was applied to define the coupled cavity modes (i.e., the modes resulting from shaker excitation). For these transfer functions, the input signal was the input force, measured with the force gauge. To determine the uncoupled cavity modes, the input signal for the transfer functions was the acoustic pressure measured at the interior reference microphone.

Based on this approach, the following modal frequencies (in Hz) were determined for the uncoupled case (interior speaker excitation):

79	238	353
102	263	381
111	284	407
154	306	432
199	332	479

Similarly, the following modal frequencies (in Hz) were determined for the coupled case (shaker excitation):

79	165	362
88	183	395
98	212	426
105	228	459
110	256	470
120	303	490
129	332	

For each modal frequency, the sound pressure level distribution was mapped from the response microphone data. Sample spatial pressure plots for the uncoupled mode at 102 Hz and the coupled mode at 105 Hz are presented in Figures 11 and 12, respectively. In these figures the view of the cabin cross-section is facing forward, so that the

excitation is at the lower right corner of the figure for uncoupled modes, and on the left side for coupled modes.

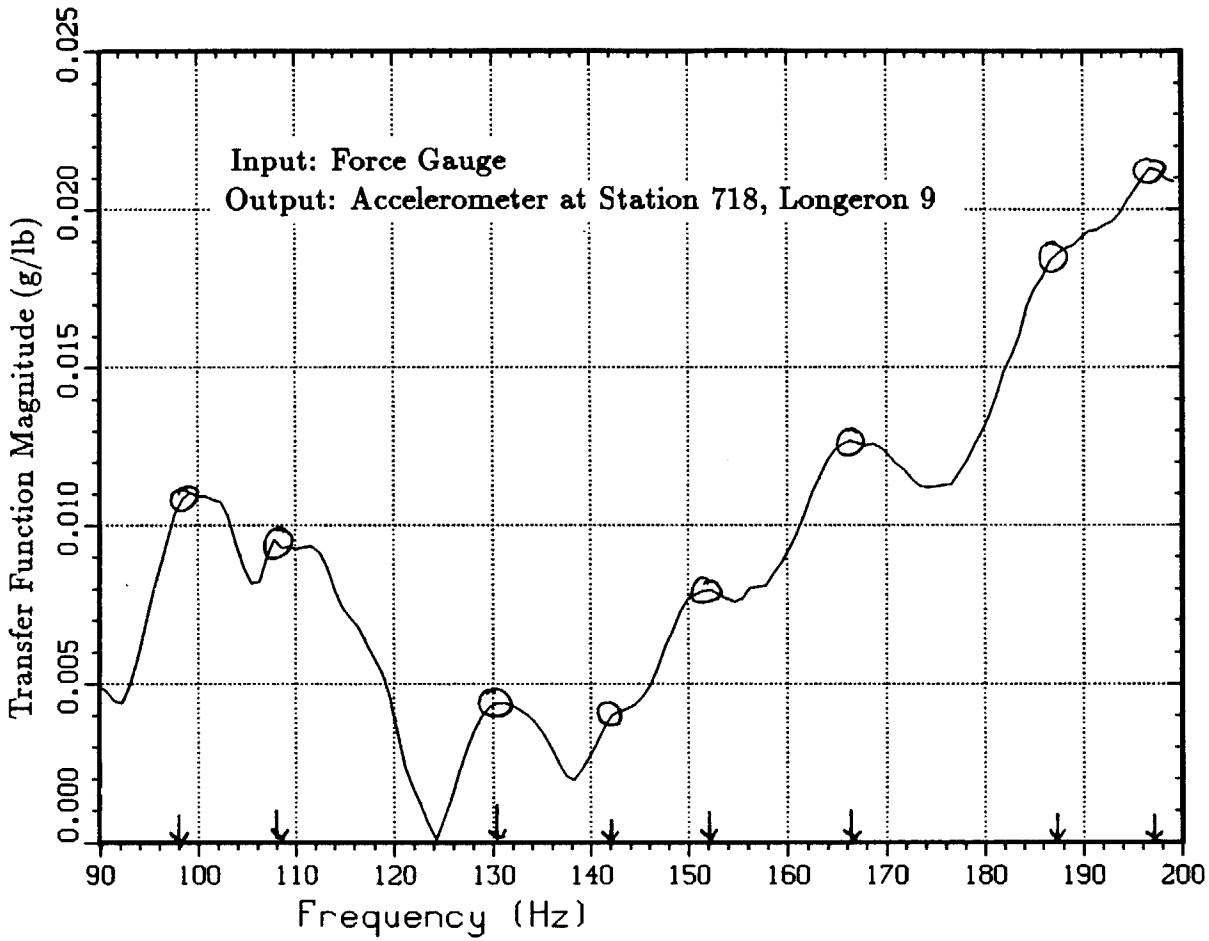

Figure 8. Frame Acceleration Transfer Function for Shaker Excitation

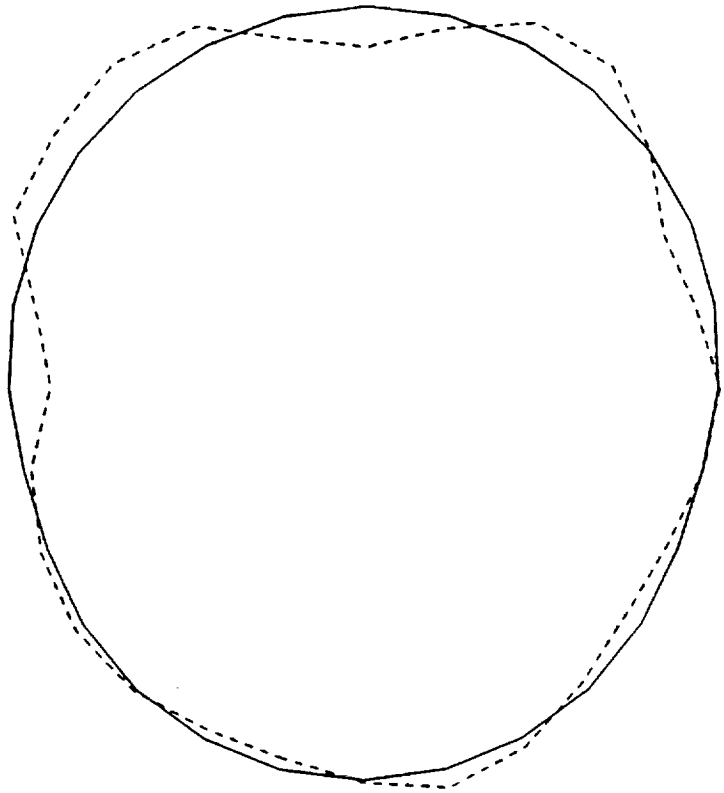

95 Hz

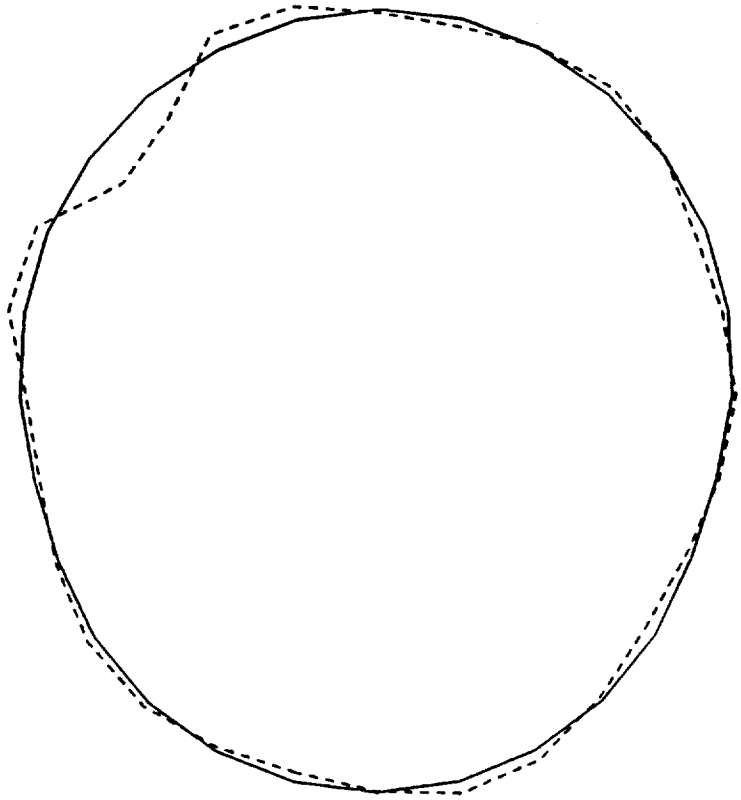

108 Hz

Figure 9. Sample Frame Modes, Station 718

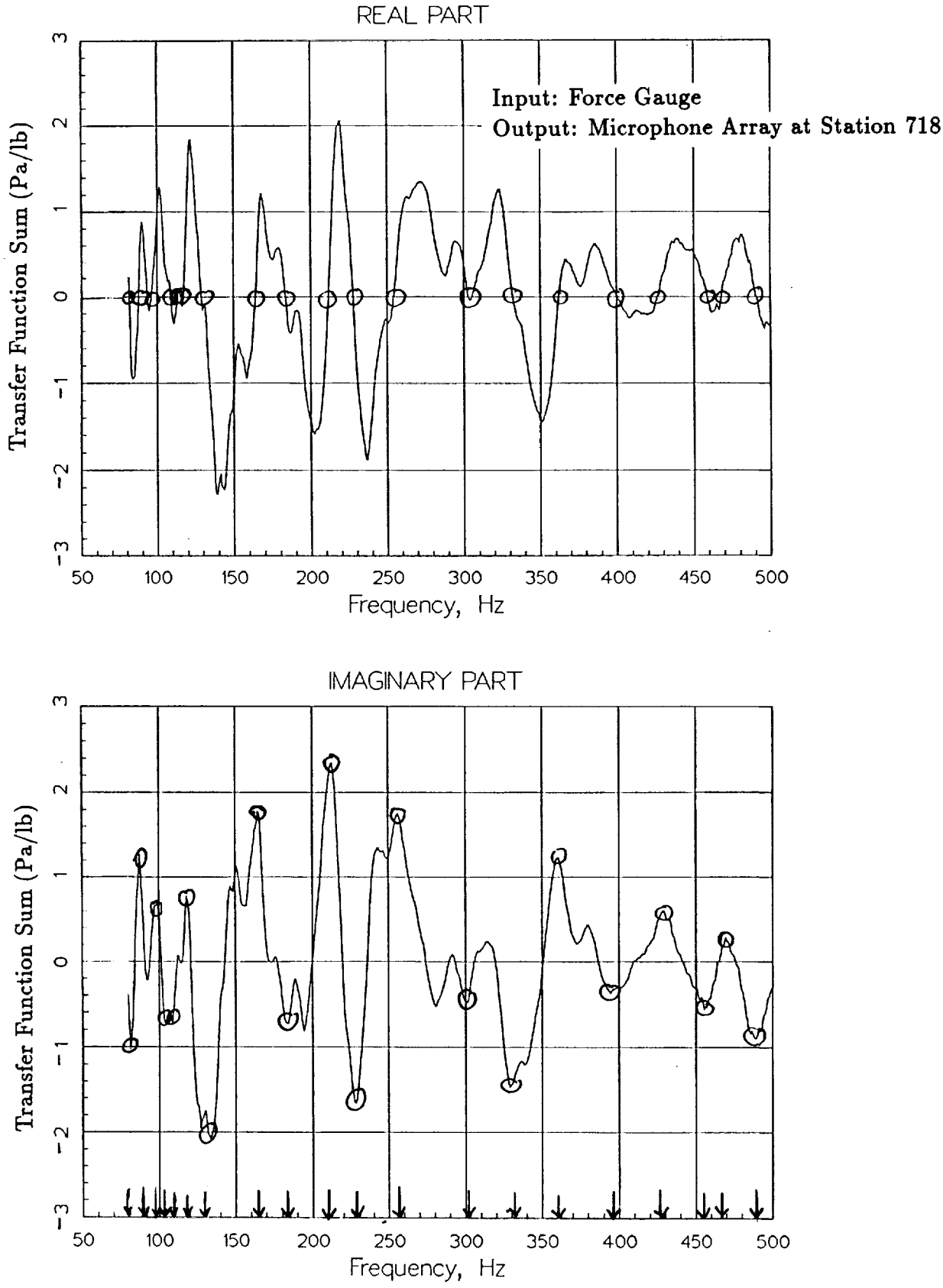

Figure 10. Cavity Pressure Transfer Function for Shaker Excitation

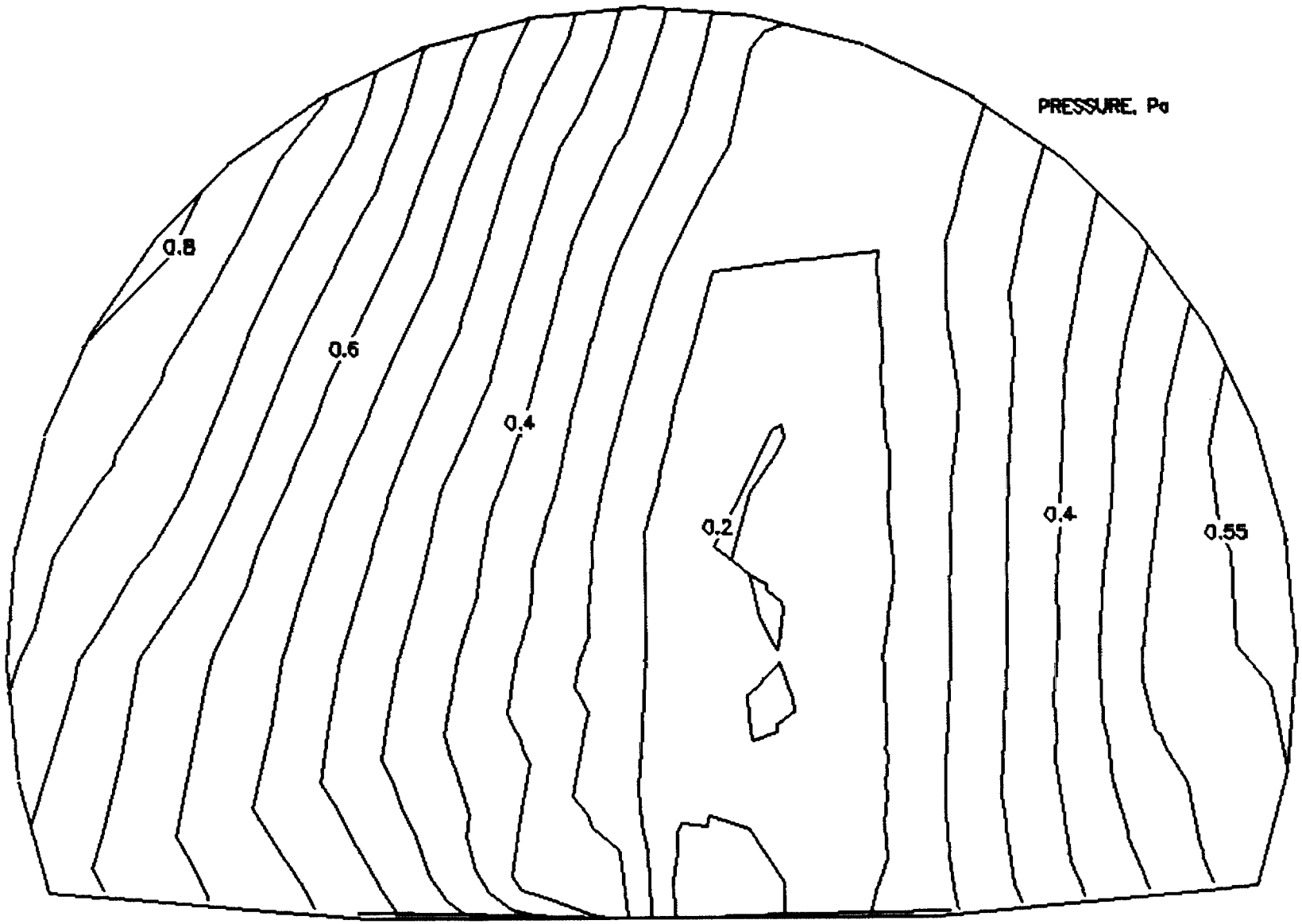

Figure 11. Sample Uncoupled Cavity Mode at Station 718 (102 Hz)

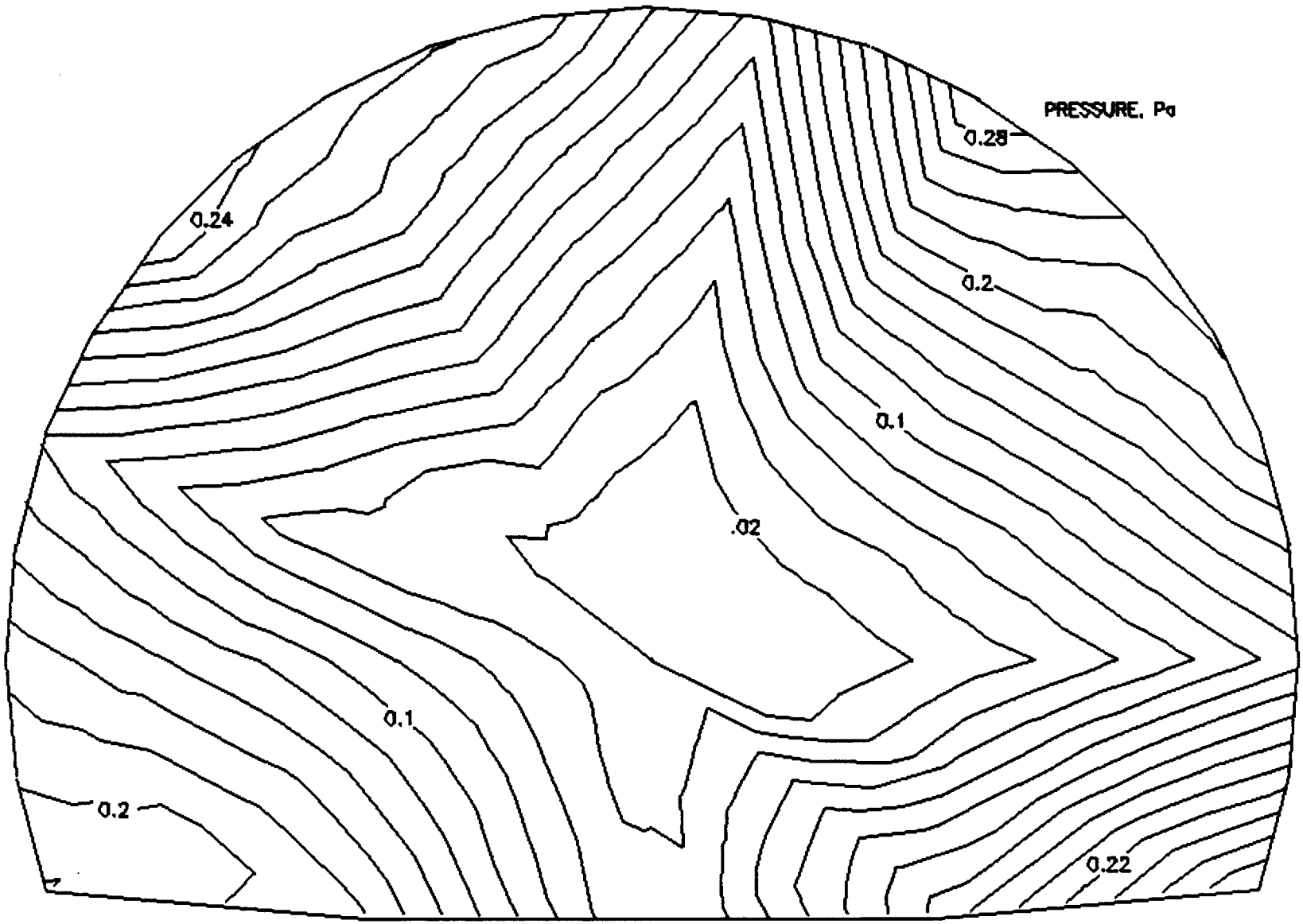

Figure 12. Sample Coupled Cavity Mode at Station 718 (105 Hz)

4 Structural-Acoustic Coupling Characteristics

The sound transmission and radiation characteristics of aircraft fuselage structures are strongly dependent on the structural-acoustic coupling inside the shell [3,4]. Dispersion diagrams or k–ω plots for both structural and cavity modes are very useful in examining and understanding such coupling phenomenon. A brief introduction to wavenumber (or k-space) analysis of structural-acoustic coupling is first presented for a uniform cylindrical shell. The results of analytical and experimental investigations for the FARF fuselage are then discussed.

4.1 Wavenumber Analysis for Cylindrical Shell

The flexural wave motion in a uniform cylindrical shell can be characterized by axial (or longitudinal) and circumferential wavenumbers, k_a and k_c. The non-dimensional wavenumber functions, $\hat{k}_a$ and $\hat{k}_c$, for the structural vibration of an idealized cylindrical shell are [5]:

$$\hat{k}_a = k_a \left(\frac{h^2 R^2}{12(1-\mu^2)} \right)^{\frac{1}{4}}$$

$$\hat{k}_c = k_c \left(\frac{h^2 R^2}{12(1-\mu^2)} \right)^{\frac{1}{4}}$$

where $k_a = \left(\frac{m\pi}{L}\right)$ and $k_c = \left(\frac{N}{R}\right)$, and m is the axial mode number, N is the structural circumferential mode number, R and L are the radius and length of the cylinder respectively, and μ is the Poisson ratio. The formula for natural frequencies of a cylindrical shell can be expressed in the following form [5]:

$$\omega_{mN} = \left((\hat{k}_a^2 + \hat{k}_c^2)^2 + \frac{\hat{k}_a^4}{(\hat{k}_a^2 + \hat{k}_c^2)^2} \right)^{\frac{1}{2}} \omega_r$$

where ω_r is the ring frequency of the cylinder. The non-dimensional wavenumber diagram of a cylindrical shell is presented in Figure 13. This figure shows lines of constant non-dimensional frequency $\left(\frac{\omega}{\omega_r}\right)$ plotted in the positive quadrant of the wavenumber functions $\hat{k}_a$ and $\hat{k}_c$. These wavenumber diagrams can also be plotted for the range of wavenumbers: -$\hat{k}_a$ to +$\hat{k}_a$ and -$\hat{k}_c$ to +$\hat{k}_c$, which results in a "figure 8" pattern [6]. The figure 8 defines a locus of wavenumbers that dominate the vibration of the shell.

The acoustic modes of a rigid-walled cylindrical waveguide take the following form [7]:

$$p_{mn}(r,\phi,z) = P_{mn}\frac{sin}{cos}(n\phi)J_n(k_r r)cos(k_z z)$$

where J_n is the Bessel function, m is axial mode order, n is the acoustic circumferential mode order, P_{mn} is pressure amplitude, and (r,ϕ,z) denote a cylindrical coordinate system. The radial wavenumber k_r is determined by the zero normal-particle wall boundary condition as characteristic solutions k_r^{np} of the equation:

$$\left[\frac{\partial J_n(k_r r)}{\partial r}\right]_{r=R} = 0$$

where n indicates the number of diametral pressure nodes and p the number of concentric circular pressure nodes (radial mode order).

The axial and radial wavenumbers satisfy the acoustic wave equation:

$$k_z^2 + (k_r^{np})^2 = k^2$$

which gives the dispersion relationship for the cylindrical cavity. The axial (k_a) and circumferential (k_c) wavenumbers and the modal frequencies for the cylindrical cavity are given by:

$$k_a = (k_z)\,|_{z=L} = \frac{m\pi}{L}$$

$$k_c = (k_r^{np})\,|_{r=R} = \frac{\gamma_{np}}{R}$$

$$\omega_{mnp}^2 = (\frac{c}{2\pi})^2\left(k_a^2 + k_c^2\right)$$

where γ_{np} are characteristic solutions of the equation $[J_n'(k_r)]_{r=R} = 0$ for the cylindrical cavity.

The acoustic dispersion diagram for the hard walled cylindrical cavity is shown in Figure 14.

4.2 Wavenumber Analysis for the FARF Fuselage

Since the FARF fuselage is a complex stiffened shell and does not conform to the idealized form of a cylindrical shell, the cylindrical shell formulae could not be used to calculate the fuselage structural and cavity modes. The FARF structural and acoustic modes were determined using the Matrix Difference Equation (MDE) method [8]. This

method is a computer code developed at DAC using a finite element approach to vibration analysis. The basic simplifying assumption is that the structure is spatially periodic or repetitive, meaning that it is a longitudinal array of identical substructures. The computer code is applicable to coupled structural-acoustic models representing the fuselage structure and the air inside.

In order to understand the acoustic waveguide behavior of the FARF fuselage cavity, predictions were first made for the acoustic modes of an equivalent hardwalled, stiffened cylindrical shell. A MDE model of such a cylindrical shell was used to determine its uncoupled modal frequencies and mode shapes. The radius (R=65.8 inch) and length (L=380 inch) of the cylindrical shell cavity are the same as that of the FARF (DC-9) fuselage. The MDE model of the hardwalled cylindrical shell consisted of 20 substructures, each substructure being 19 inches long. Figure 15 shows sample predicted acoustic pressure contours for the (m=3, n=2, p=0) mode. The circumferential and radial mode ordering of these acoustic modes can be done by either comparing the predicted contours with those obtained from the classical theory for circular cylindrical shells or by identifying the modal distribution of acoustic pressures. The MDE model of the hardwalled cylindrical cavity was then modified to represent a flexible wall cylindrical shell, in order to determine the coupled modal frequencies and mode shapes for the cylinder.

The structural-acoustic coupling phenomenon can be studied using wavenumber matching [3] or mode matching [4] techniques. Both require matching the acoustic and structural mode (or wavenumber) and imply that only the modes of the same axial and circumferential orders can couple. Although the coupled acoustic and structural modes differ from the respective uncoupled modes, they may be assumed to resemble closely their uncoupled components for the purposes of approximate analysis [3]. Hence the acoustic and structural dispersion diagrams may be superimposed to locate possible structural-acoustic interactions.

The acoustic and structural dispersion diagrams for uncoupled modes of the cylindrical shell are shown superimposed in Figure 16. For a given circumferential mode order, equality of axial wavenumber (or mode order) then gives the coincidence condition. At coincidence, optimum conditions exist for transfer of energy between these modes. The mode coupling would occur where structural and acoustic dispersion curves coincide or cross each other for the same axial and circumferential mode order. Figure 16 indicates that the coincidence between the lower-order circumferential shell modes (e.g. N=0 and 1) and the lower-order circumferential acoustic modes (e.g. n=0 and 1) and low radial order (p=0), can occur at frequencies close to the acoustic mode cutoff frequencies. For example, the lowest possible coincidence frequency is due to the coupling between the (m=1, N=1) structural mode and the (m=1, n=1, p=0) acoustic mode which corresponds to the cutoff frequency of this acoustic mode. Between this

frequency and the ring frequency, there can be several such coincidences; any one shell mode can be coincident with all the acoustic modes of equal circumferential order (n) and increasing radial order (p). Multiple coincidences between the lower order structural and acoustic curves may also occur since portions of these curves run parallel to each other (e.g. the N=0 structural curve and the (n=0, p=4) acoustic curve). The chance of coincidence for the higher order shell modes (N = 4 and above), however, becomes less as the structural curves tend to rise rapidly and run parallel to the lower order acoustic curves.

The structural and acoustic cavity modes of the FARF fuselage were then determined using the MDE method. The MDE model of the FARF fuselage consisted of 20 substructures. Each substructure is 19 inches long and represented one bay between frames. Every longeron was represented, as well as the floor and floor-support struts. Figure 17 shows the cavity spatial pressures predicted at 118 Hz. This predicted (n=2, p=0) acoustic mode compares very well with the measured cavity mode at 105 Hz (see Figure 12). The difference in frequencies is likely due to the simplified model used for predictions.

The predicted structural and acoustic dispersion curves for the fuselage are shown in Figure 18. These dispersion curves, particularly for the lower-order modes, appear to be very similar to those obtained for the equivalent cylindrical shell. It may be observed from Figure 18 that structural-acoustic coupling can occur for the (1,1) structural mode and the (1,1,0) acoustic mode, in the frequency range from 60 to 70 Hz (below the frequency range measured during the test program). The figure also shows that structural acoustic coupling may occur for the (3,2) structural mode and the (3,2,0) acoustic mode, in the frequency range from 120 to 150 Hz. Coupling of other structural and acoustic modes appears unlikely, since no other coincidences of structural and acoustic dispersion curves of the same axial and circumferential mode orders are shown in the figure.

4.3 Experimental Results

The wavenumber spectrum analysis approach was used to examine the structural-acoustic coupling for the FARF fuselage, between the (3,2) structural mode and the (3,2,0) acoustic mode. The spatial domain data for the vibration response was obtained using the 13x15 array of accelerometers mounted on the left side of the fuselage (see Figure 6). The interior sound field was mapped using a three-dimensional array of microphones, comprised of the microphones in a ring around the periphery of the cabin adjacent to the sidewall (i.e., ring 5 on Figure 7), at each of 13 stations within the cabin. The k-space vibration response was obtained by implementing two-dimensional spatial Fourier transforms (at each temporal frequency) on the spatial domain data. Using the

cylindrical coordinate system, the k-space acceleration spectrum may be represented as follows [6]:

$$\ddot{W}_N(R, k_z, \omega) = \frac{1}{2\pi} \int_{-\infty}^{\infty} \int_0^{2\pi} \ddot{w}(R, \phi, z, \omega) e^{-i(k_z z + N\phi)} dz d\phi$$

where $\ddot{w}(R, \phi, k_z, \omega)$ is the spatial acceleration response on the cylinder surface, R is the radius of the shell, and N is the structural circumferential mode number.

The k-space acoustic pressure, $P_{mn}(r, k_z, \omega)$, at a constant radial location inside the fuselage may be similarly defined. The circumferential wavenumbers and mode orders of the structural and acoustic cavity modes are related by the following relationships: $k_c = \mathrm{N/R}$ for the structural mode and $k_r^{np} = \frac{\gamma_{np}}{r}|_{r=R}$ for the acoustic cavity mode, where n and p are circumferential and radial mode numbers for acoustic modes respectively. The axial mode numbers may also be calculated from the axial wavenumbers using $k_a = \frac{m\pi}{L}$. Since $P_{mn}(r, k_z, \omega)$ and $\ddot{W}_N(R, k_z, \omega)$ are complex functions, only the magnitude of these functions will be shown in the form of contour plots.

The k-space vibration reponse of the fuselage at 105 Hz due to the shaker broadband excitation is shown in Figure 19. The k-space acoustic response of the FARF cavity at the same frequency obtained from the ring 5 array of microphones is shown in Figure 20. (Note the "figure 8" pattern of these wavenumber diagrams.)

It may be observed in Figure 19 that a number of structural modes (N=2 to 7, calculated using the equation above) contribute to the response of the FARF structure at 105 Hz. The acoustic modes contributing to the FARF cavity response are found (Figure 20) to be in the range of n=1 to 3 with the n=2 mode being the most dominant. Although the N=2 structural mode is not resonant at 105 Hz, it has spatial contribution at this frequency and shows up with somewhat diminished amplitude in the vibration wavenumber plot. It therefore appears from Figures 19 and 20 that the N=2 structural mode is coupling with the n=2 acoustic mode, in agreement with the earlier predictions.

This example illustrates the usefulness of the wavenumber analysis approach for defining the modal characteristics of the fuselage and for understanding the structural-acoustic coupling of the shell and cavity.

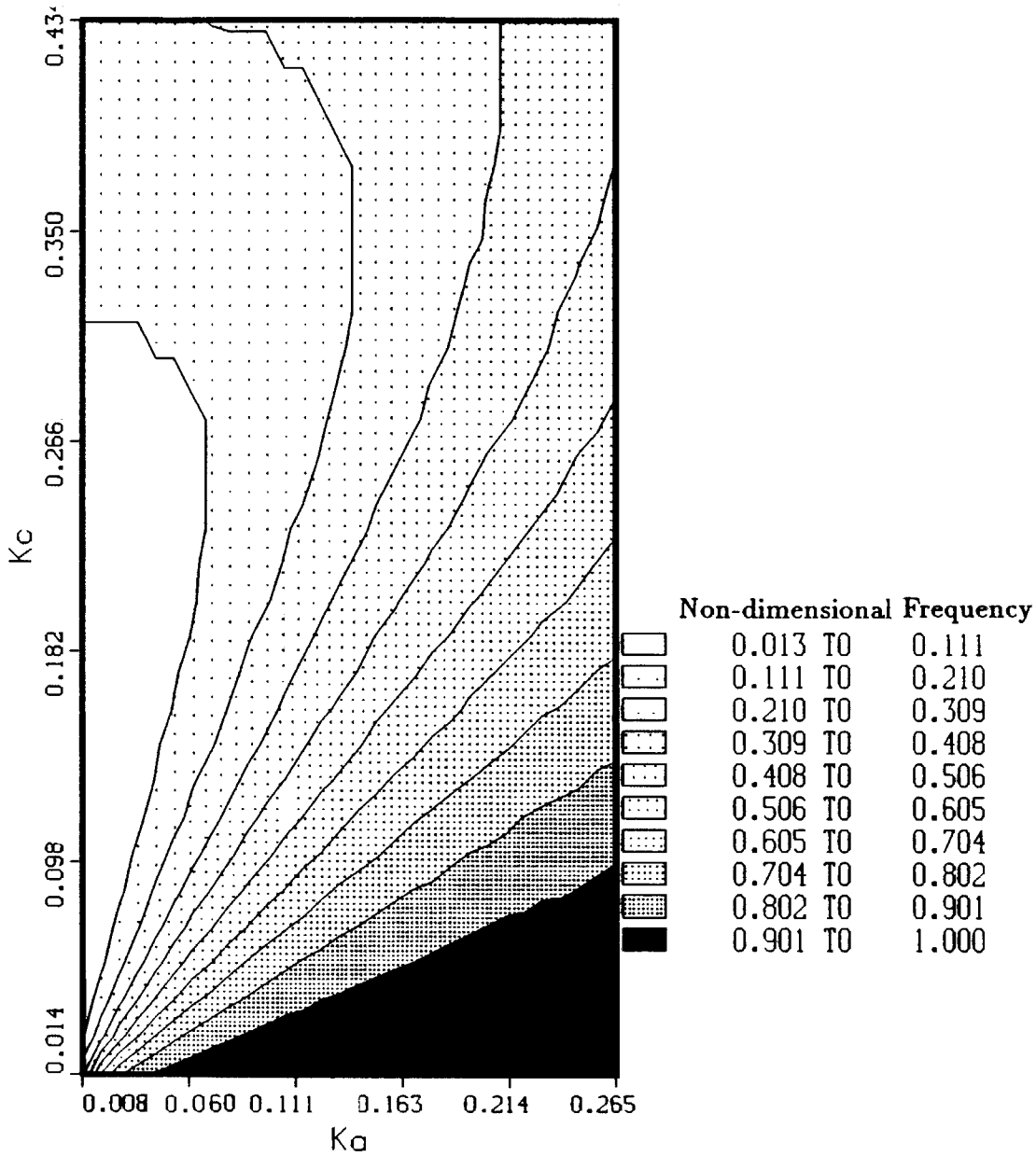

Figure 13. Wavenumber Diagram For a Cylindrical Shell (Non-dimensional)

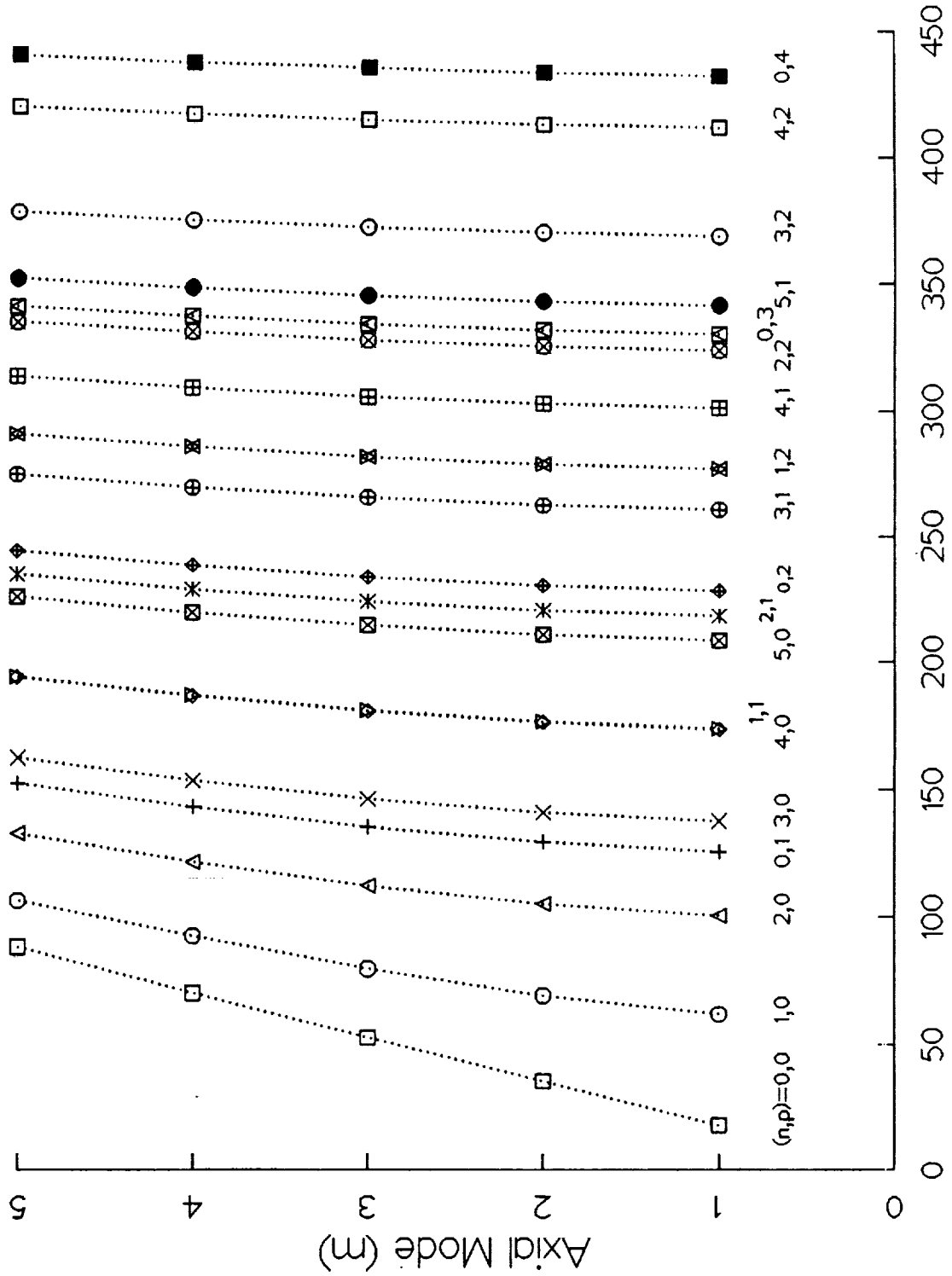

Figure 14. Acoustic Dispersion Curves for a Cylindrical Cavity

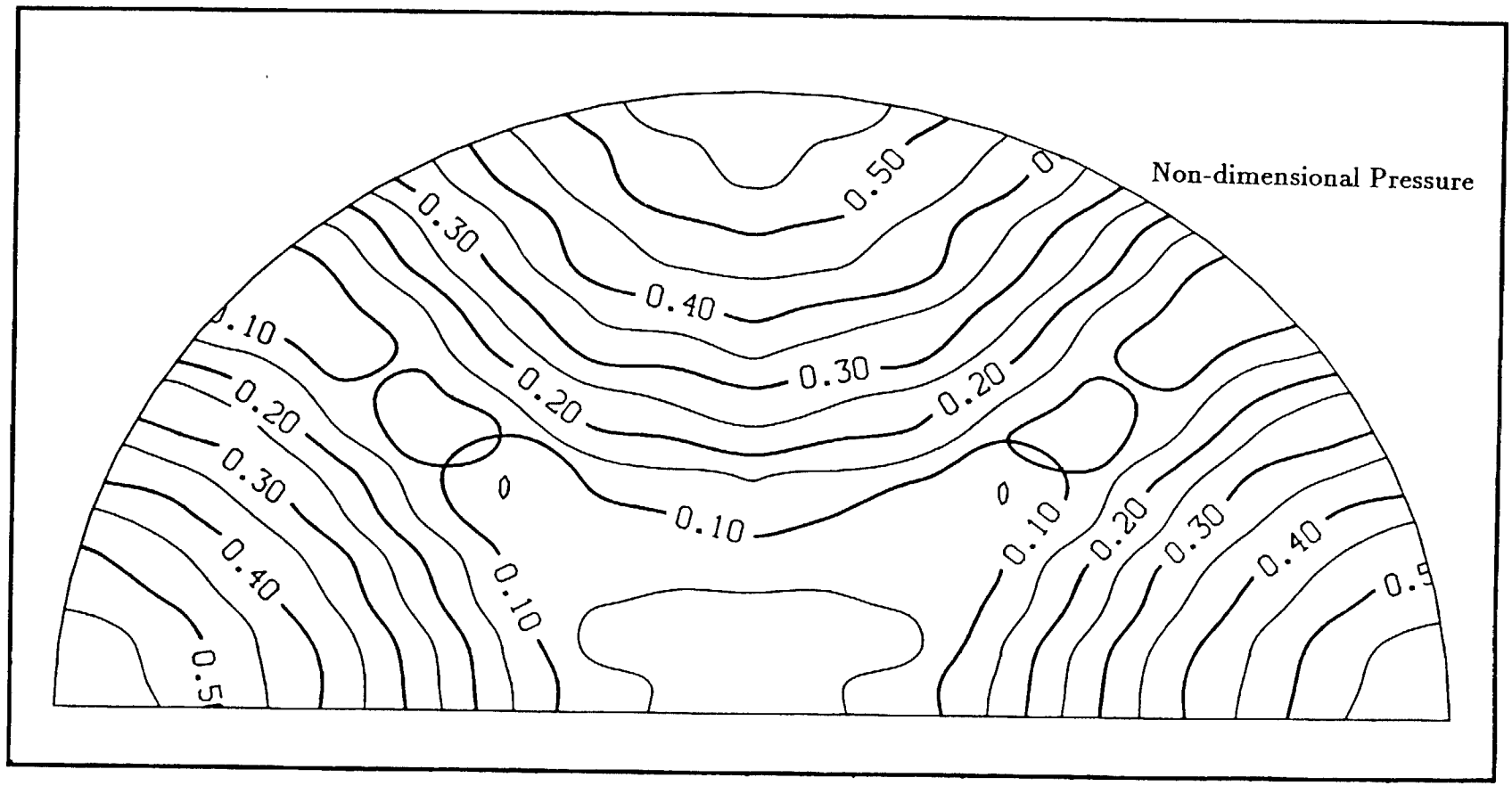

Figure 15. Predicted Uncoupled (m=3, n=2, p=0) Mode for a Cylindrical Cavity

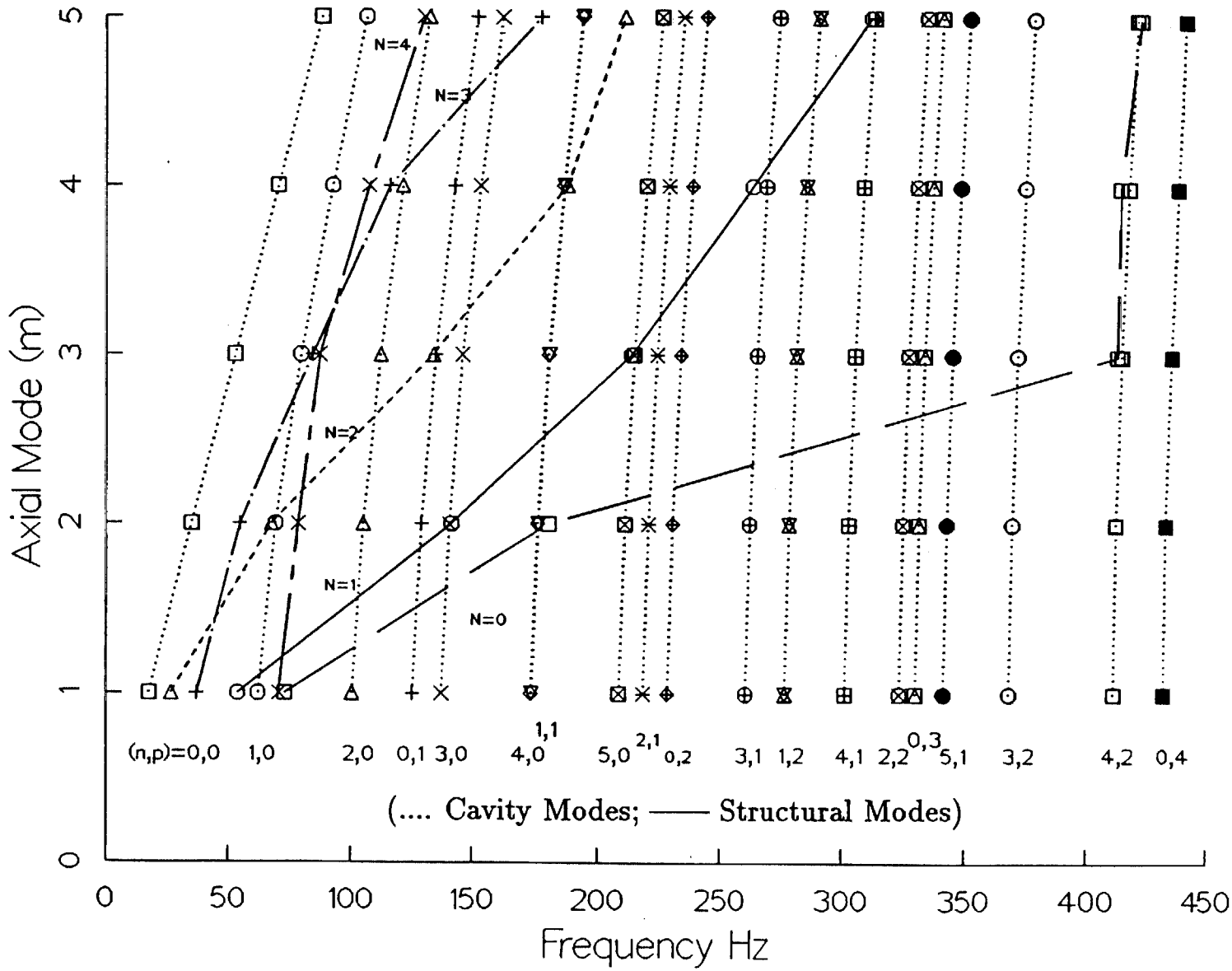

Figure 16. Dispersion Curves for Identifying Coupled Modes for a Cylindrical Shell

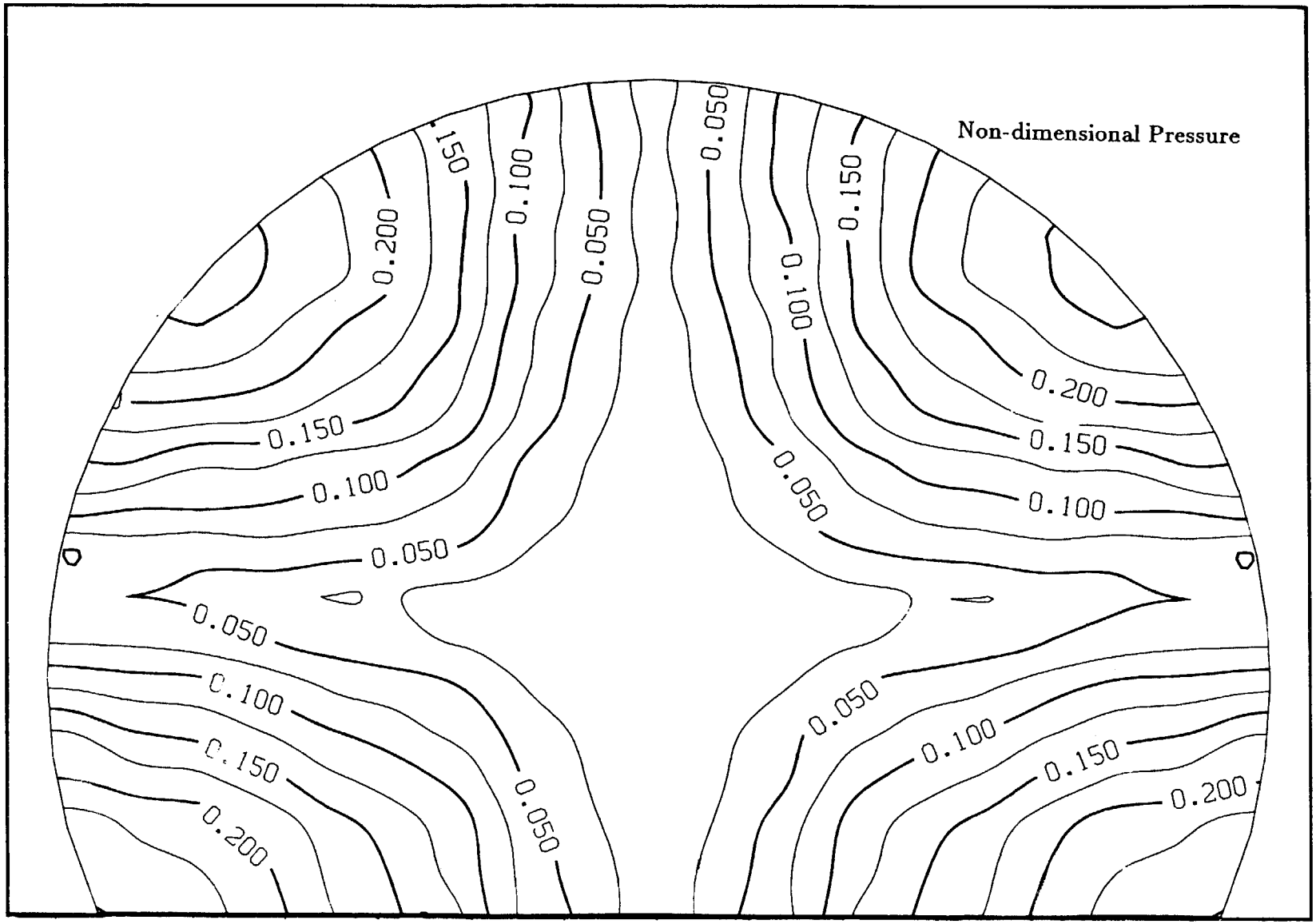

Figure 17. Predicted Coupled (n=2, p=0) Mode for the FARF Cavity at 118 Hz

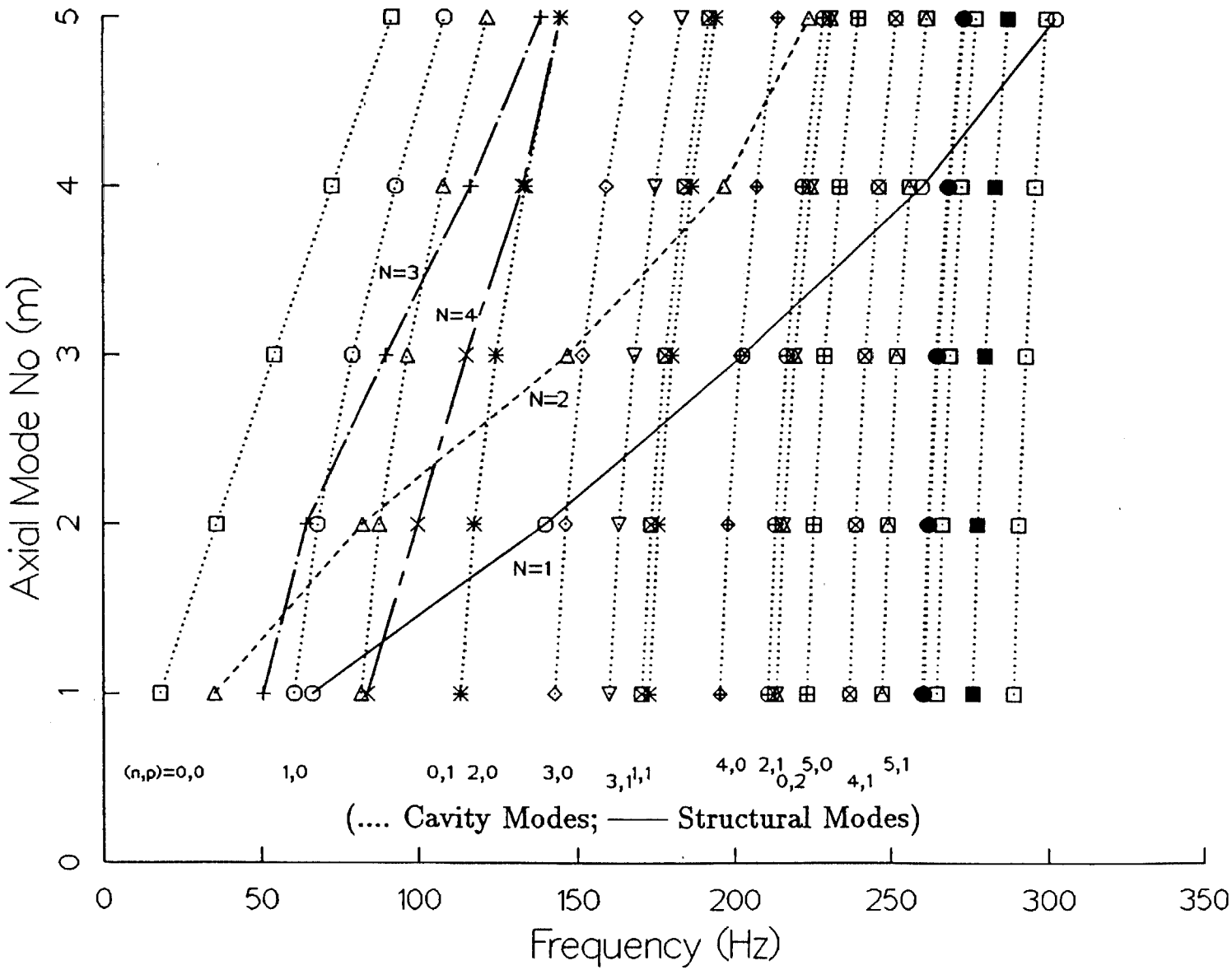

Figure 18. Dispersion Curves for Identifying Coupled Modes for the FARF Fuselage

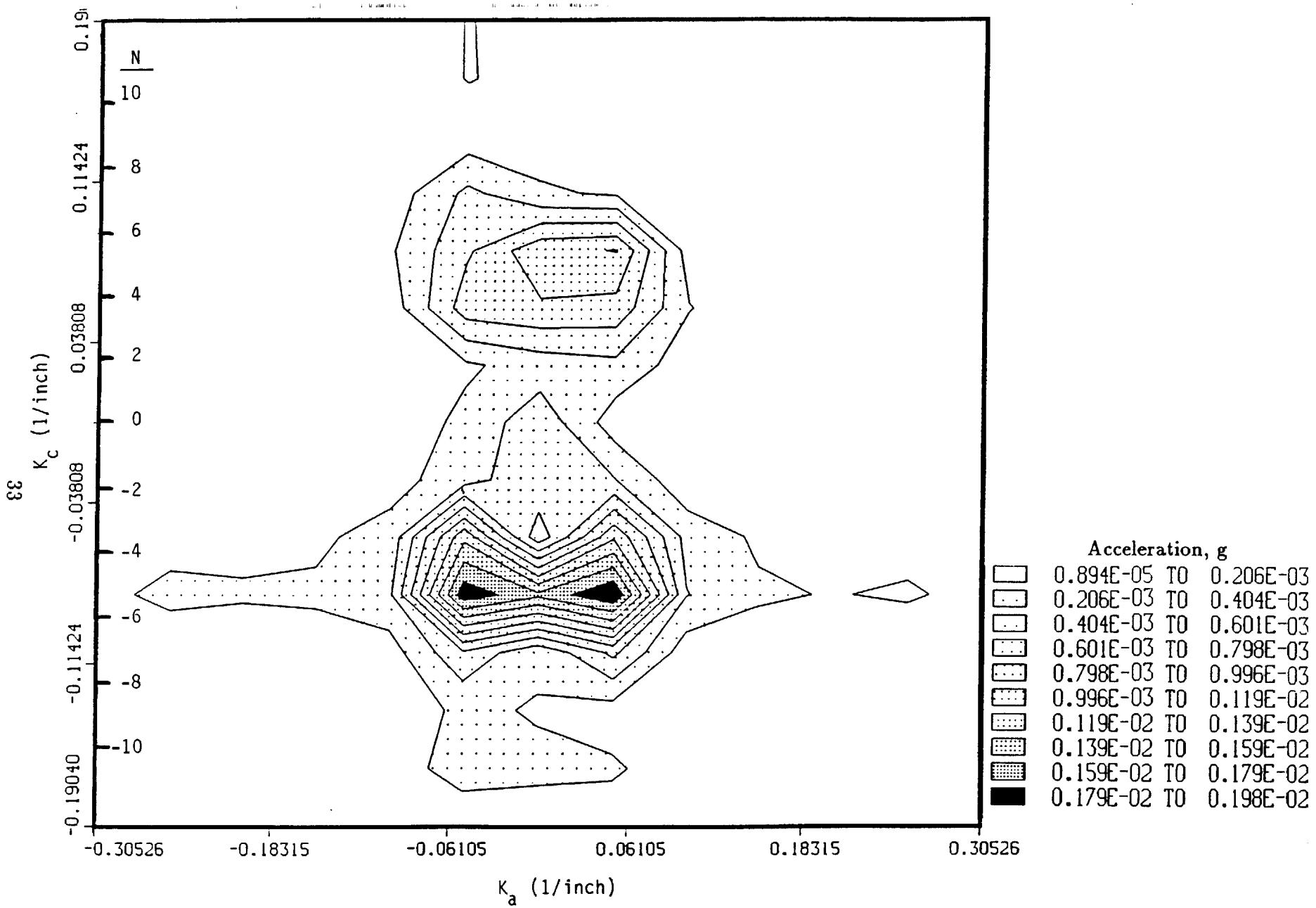

Figure 19. Acceleration Wavenumber Map for Shaker Broadband Excitation, 105 Hz

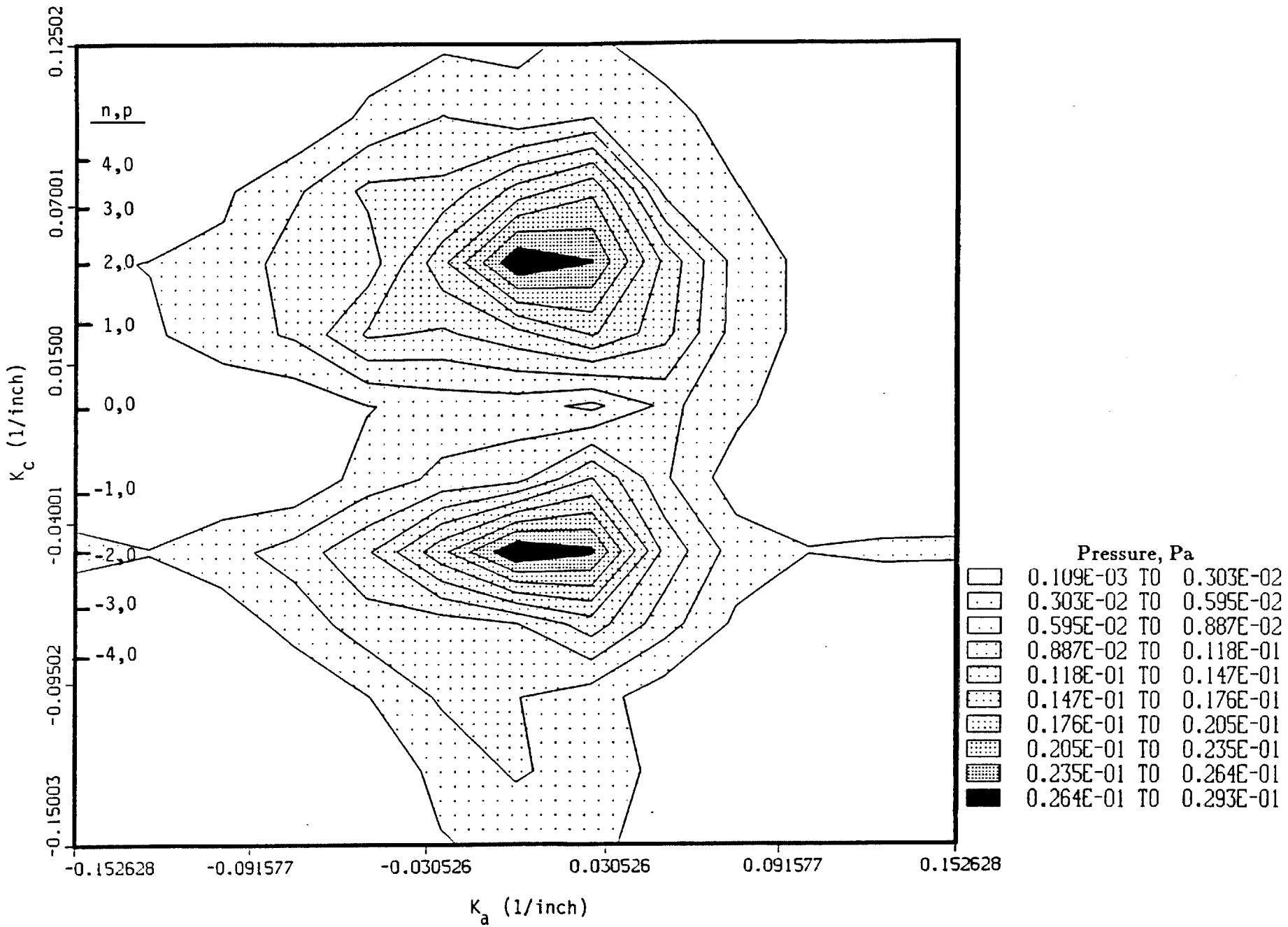

Figure 20. Pressure Wavenumber Map for Shaker Broadband Excitation, 105 Hz

5 Response to Acoustic and Vibration Excitation

In this section, the measured response of the test fuselage to various types of excitations is reviewed. Fuselage response is examined in terms of the interior acoustic pressure, using spatial plots and wavenumber maps for selected frequencies and excitation conditions.

5.1 Shaker vs. Speaker Excitation

The spatial distribution of acoustic pressure within the cabin at station 718 resulting from shaker broadband excitation is shown in Figure 21, for three frequencies (125, 168, and 250 Hz). The corresponding spatial plots for the same frequencies resulting from broadand acoustic excitation from a single exterior loudspeaker is shown in Figure 22. (Note that for Figure 21 the shaker is located on the right side of the fuselage, while for Figure 22 the speaker is located on the left side of the fuselage.) While the mechanical and acoustic excitations clearly cause distinctly different cabin pressure distributions, no specific trends with either frequency or excitation type can be discerned from the plots in Figures 21 and 22.

In Figures 23 and 24, the wavenumber maps determined from the ring 5 microphones are presented for the same three frequencies for shaker and speaker excitation, respectively. Figure 23 shows that for shaker excitation, the wavenumber pressure distributions are dominated by the n=2 mode in the circumferential direction, for all three frequencies. In contrast, Figure 24 shows that for speaker excitation, the dominant circumferential mode increases with increasing frequency, from n=2 to n=6. The wavenumber maps also show that the dominant axial modes for speaker excitation are at and around zero wavenumber (n=0) for all frequencies (Figure 24), while for shaker excitation the axial mode number increases with frequency (Figure 23).

An explanation for this behavior may be found in Figure 18. This figure shows that with increasing axial mode order the N=2 structural mode can be excited over a wide frequency range of 40-250 Hz. At the higher frequencies the point mechanical force (ideally a δ-function in the spatial domain, but white noise in k-space) can, therefore, excite the low wavenumber N=2 mode, which in turn can couple with the (n,p = 2,0 and 2,1) acoustic modes. The acoustic excitation, on the other hand, is spatially distributed over the length of the fuselage but not around the circumference. Consequently, the acoustic excitation results in excitation of lower order axial but higher order circumferential modes at higher frequencies.

Further, Figures 23 and 24 demonstrate that there are distinct differences in the fuselage response to acoustic versus mechanical excitation in both axial and circumfer-

ential directions, as reflected in the wavenumber maps. This implies that wavenumber spectral mapping of the cavity acoustic pressure may have great potential as a tool for diagnosing airborne versus structureborne transmission paths into the cabin.

5.2 Broadband vs. Tone Excitation

Figure 25 shows the cabin acoustic pressure distribution and wavenumber map at 250 Hz, for broadband acoustic excitation of the fuselage from a single loudspeaker. The corresonding spatial and wavenumber plots for acoustic excitation with a 250 Hz tone from the same loudspeaker are shown in Figure 26. Comparison of these two figures demonstrates that the response of the fuselage at a particular frequency is essentially identical under broadband and tonal acoustic excitation.

This result was not unique to excitation at 250 Hz; it was found to occur for all frequencies studied.

5.3 Tone Excitation with Wave-Trace Velocity

Figure 27 presents additional spatial and wavenumber plots corresponding to the previous two figures, for acoustic excitation from the five-speaker time-delayed array using a 250 Hz tone. Comparison of the spatial pressure distributions in Figures 26 and 27 shows that simulation of wave-trace velocity results in noticeable but small differences in acoustic pressures; the differences are more pronounced at lower frequencies (e.g., at 100 and 125 Hz). Comparison of the wavenumber maps in Figures 26 and 27 shows that for tonal excitation the wave-trace velocity excites additional, lower order circumferential modes. While these additional modes are not the dominant contributors to the acoustic pressure field, their presence modifies the distribution of noise levels within the cabin. Nevertheless, wave-trace velocity effects, as simulated in the test facility, appear to be relatively small.

5.4 Combined Shaker and Speaker Excitation

Figure 28 presents cabin acoustic pressure distributions at 125, 168, and 250 Hz for the final excitation, combined shaker and speaker broadband excitation. Similarly, Figure 29 presents wavenumber maps for the same frequencies for the combined broadband excitation. These figures may be compared with Figures 21 and 23 for shaker excitation, and Figures 22 and 24 for speaker excitation. For the input levels used in these tests the shaker excitation generally produced higher noise levels in the cabin than the speaker excitation; thus the acoustic pressure distributions and wavenumber

maps for the combined excitations at these frequencies are dominated by the shaker excitation. For selected wavenumber ranges where the shaker excitation is not dominant, the wavenumber pressures for the combined excitations appear to be the superposition of the wavenumber pressures for the individual excitations.

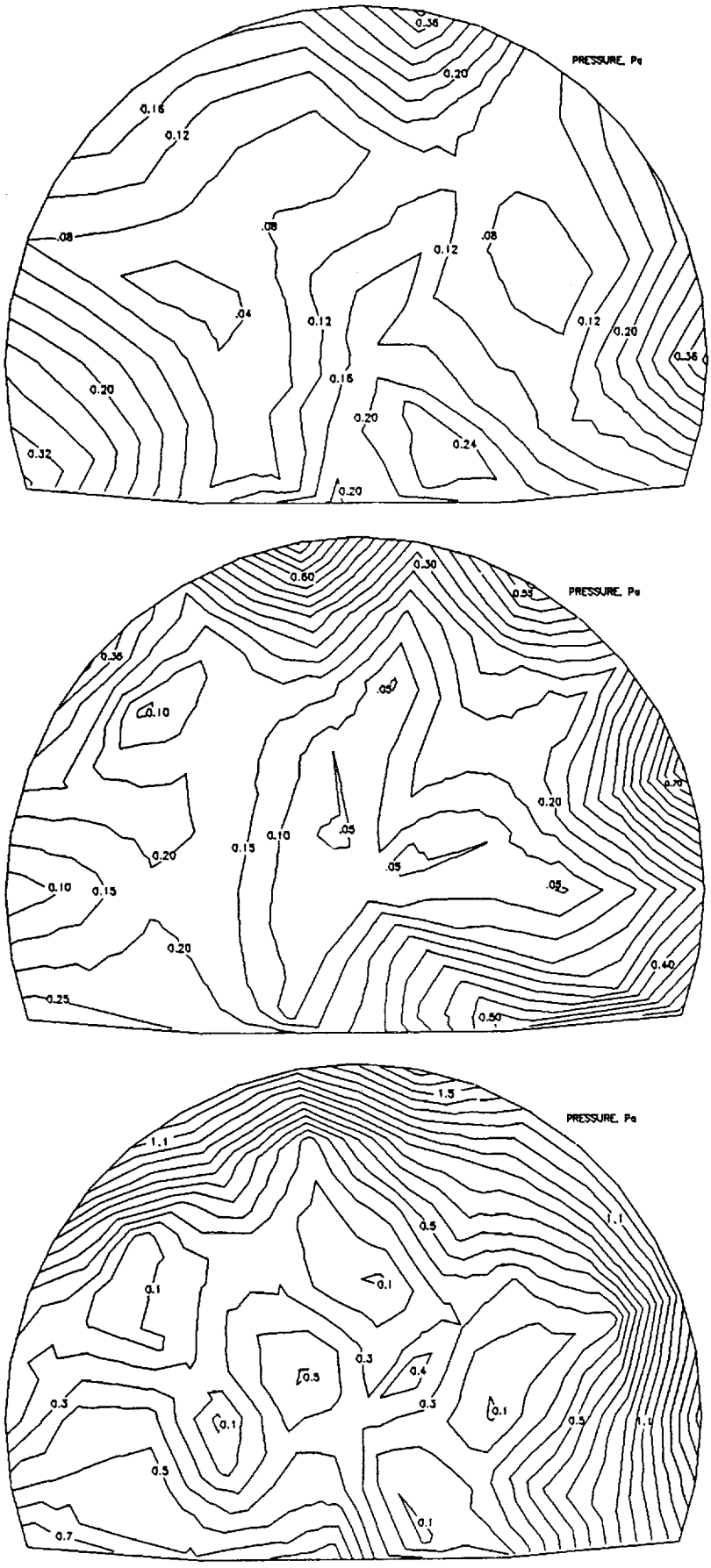

Figure 21. Cavity Pressure Distributions, Shaker Broadband Excitation

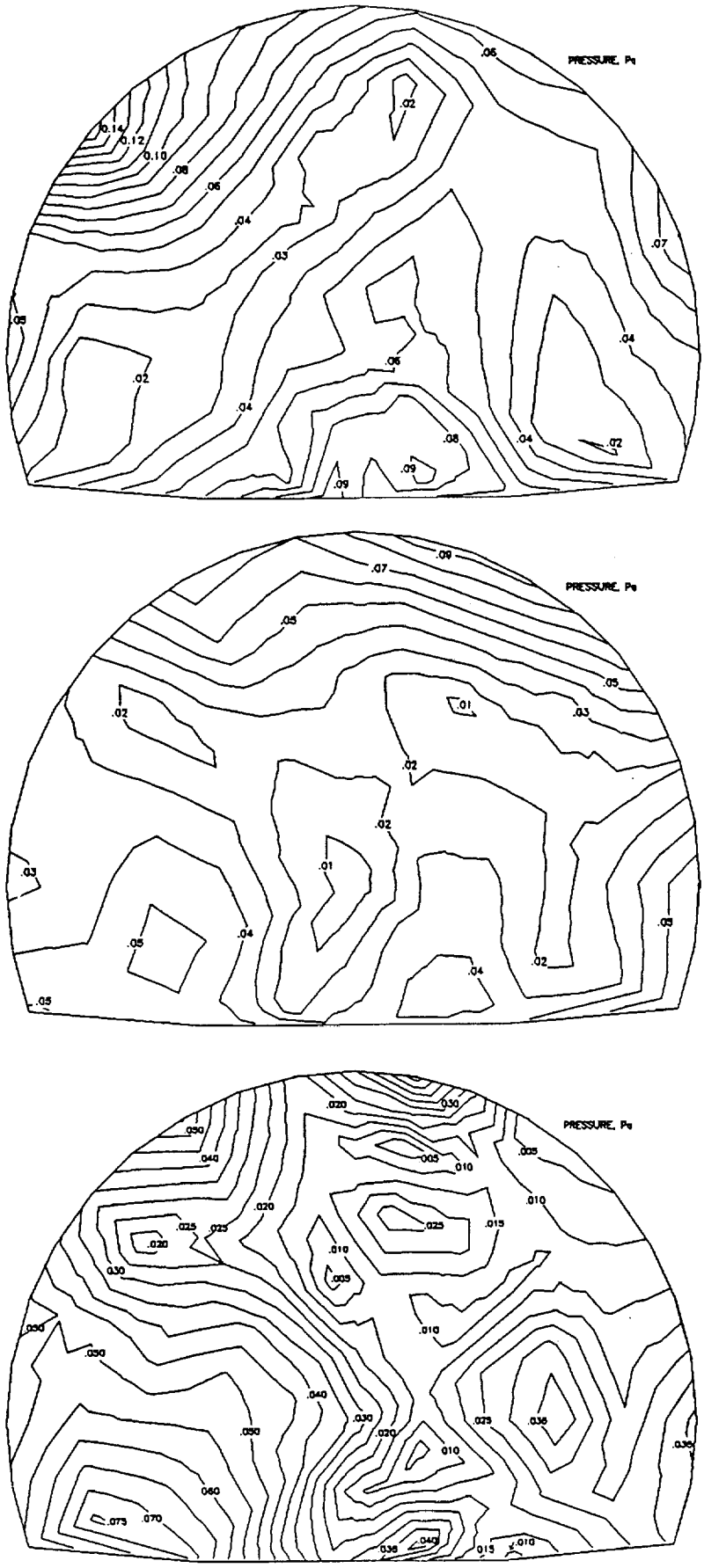

Figure 22. Cavity Pressure Distributions, Single Speaker Broadband Excitation

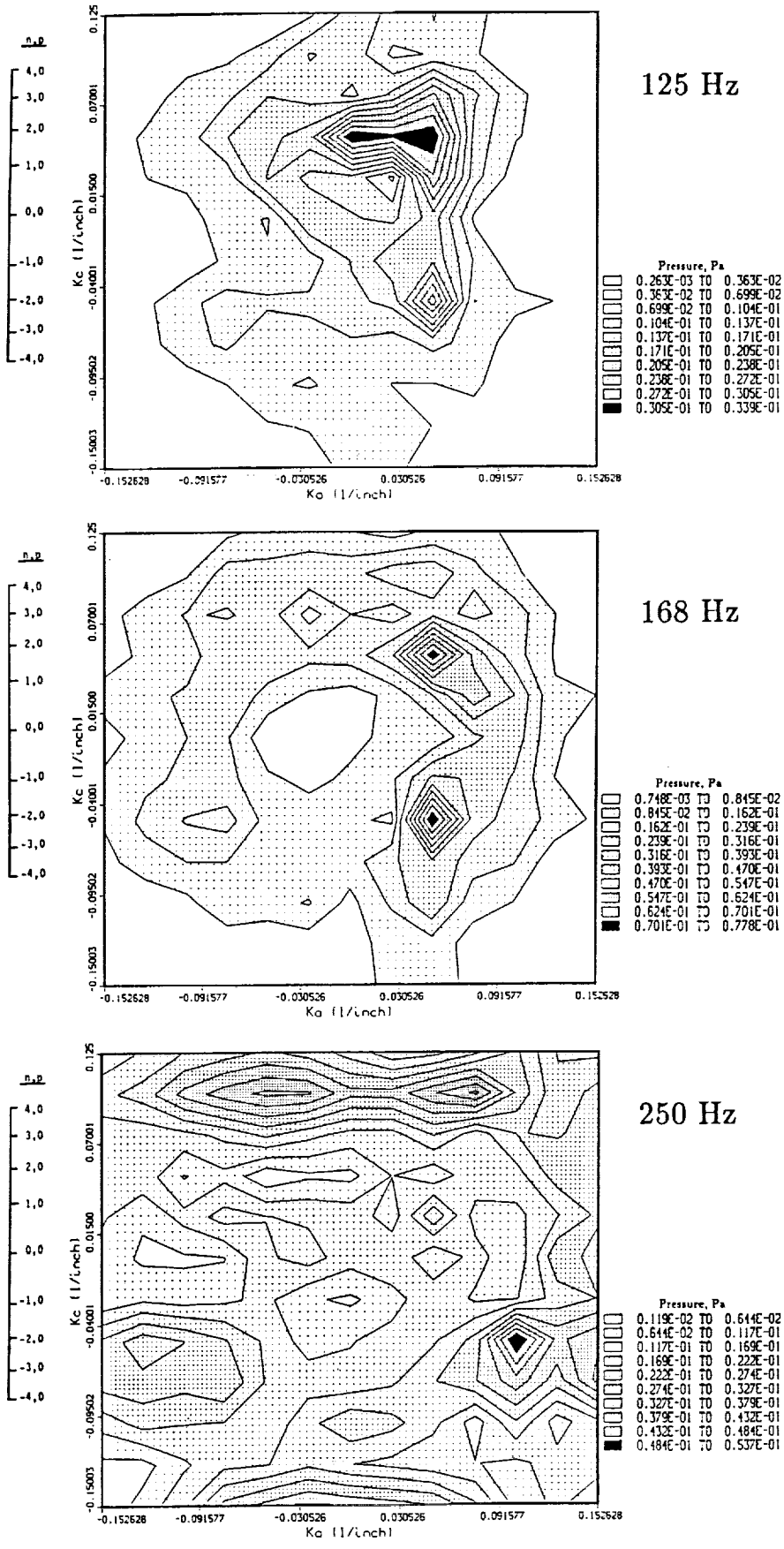

Figure 23. Pressure Wavenumber Maps, Shaker Broadband Excitation

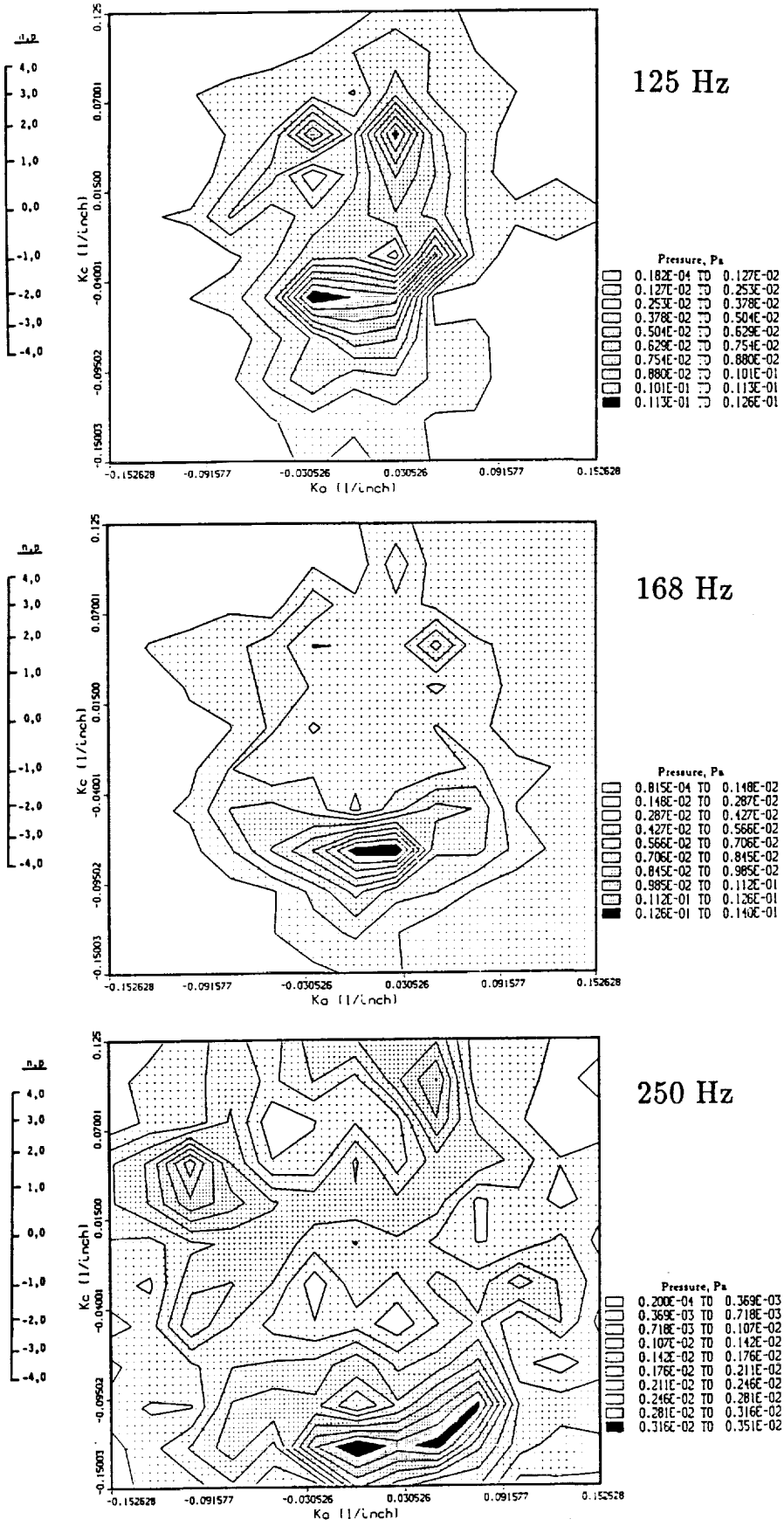

Figure 24. Pressure Wavenumber Maps, Single Speaker Broadband Excitation

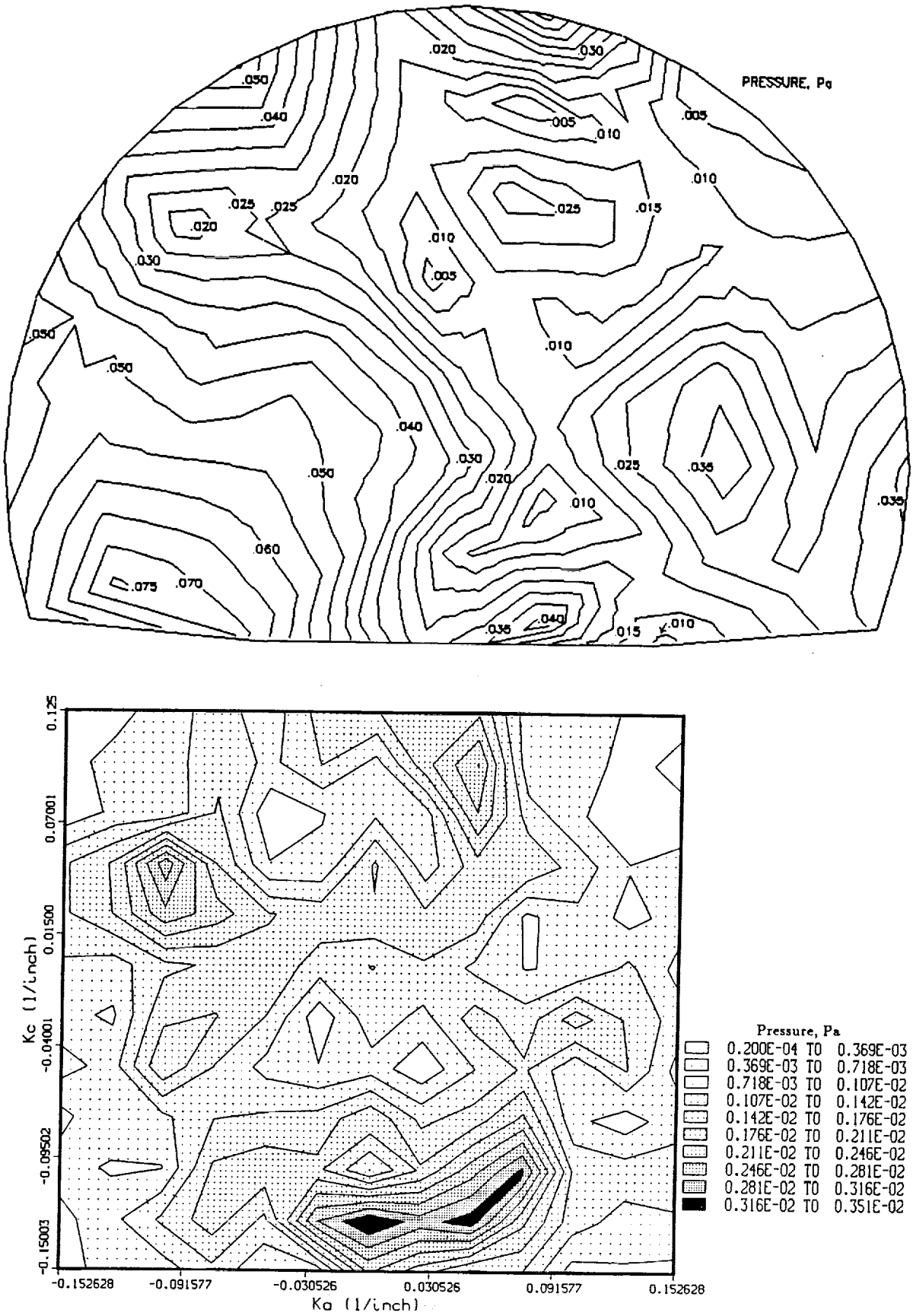

Figure 25. Cavity Pressure Distribution and Wavenumber Map for 250 Hz, Single Speaker Broadband Excitation

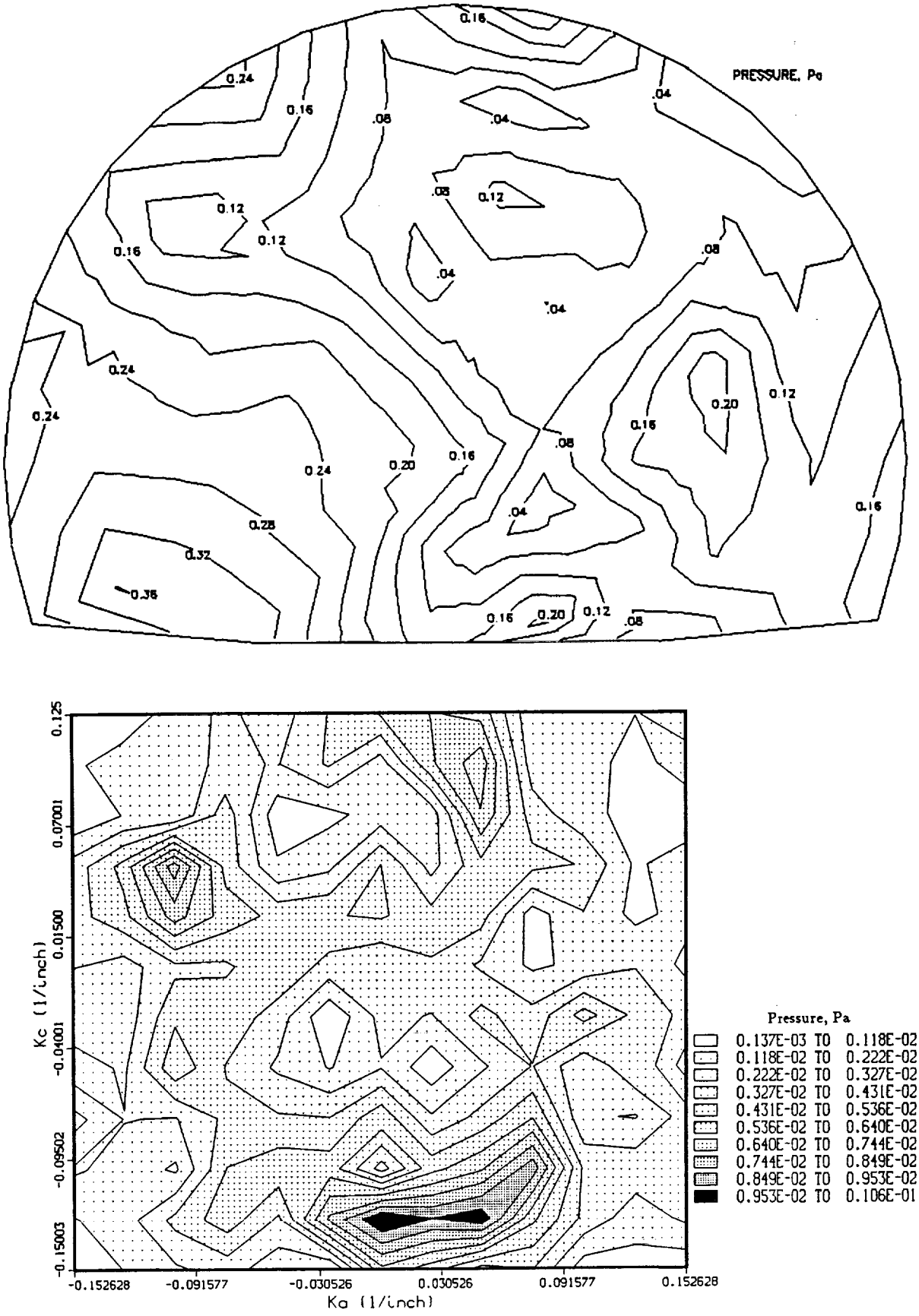

Figure 26. Cavity Pressure Distribution and Wavenumber Map for 250 Hz, Single Speaker Tonal Excitation

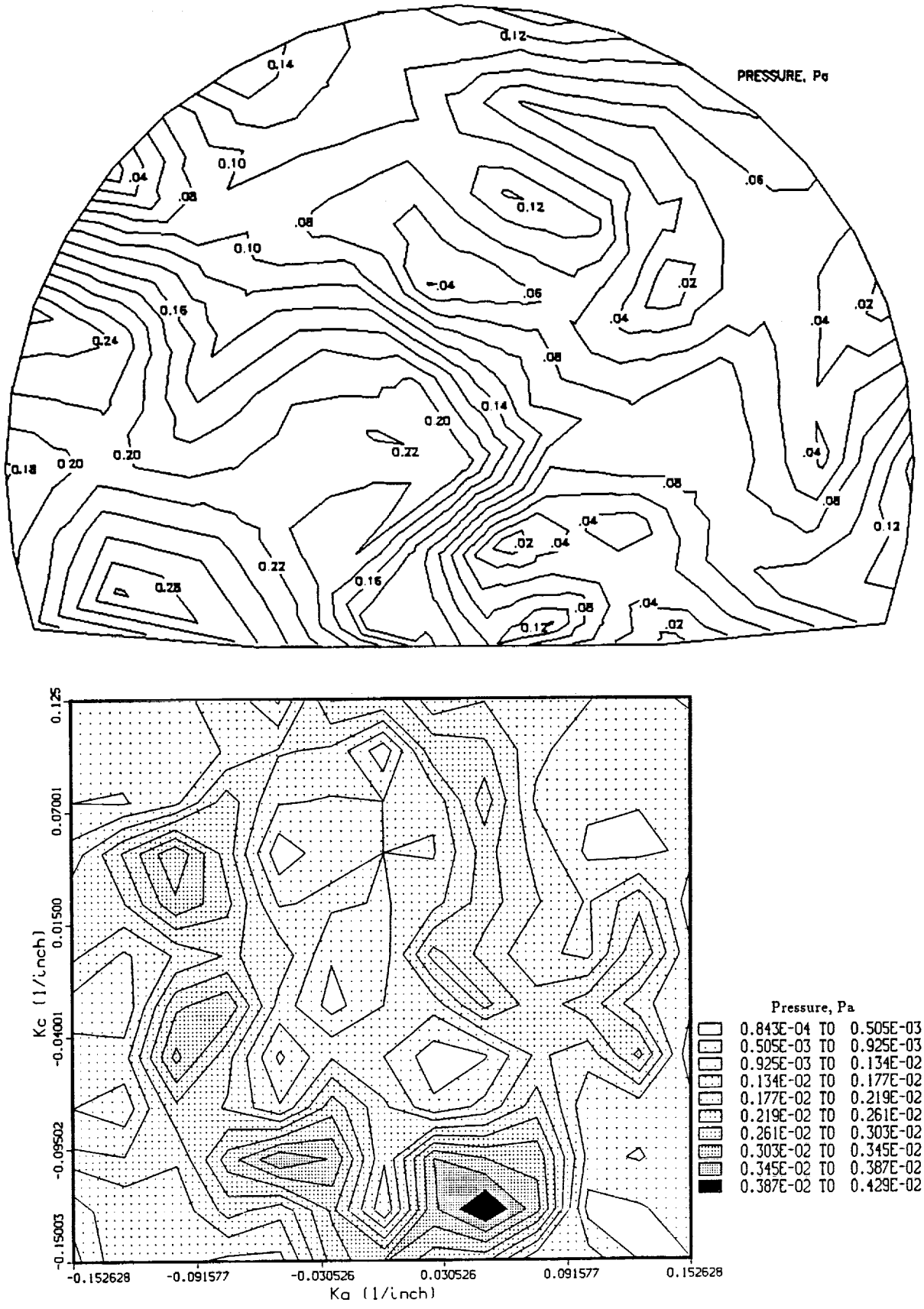

Figure 27. Cavity Pressure Distribution and Wavenumber Map for 250 Hz, Multiple Speaker Tonal Excitation

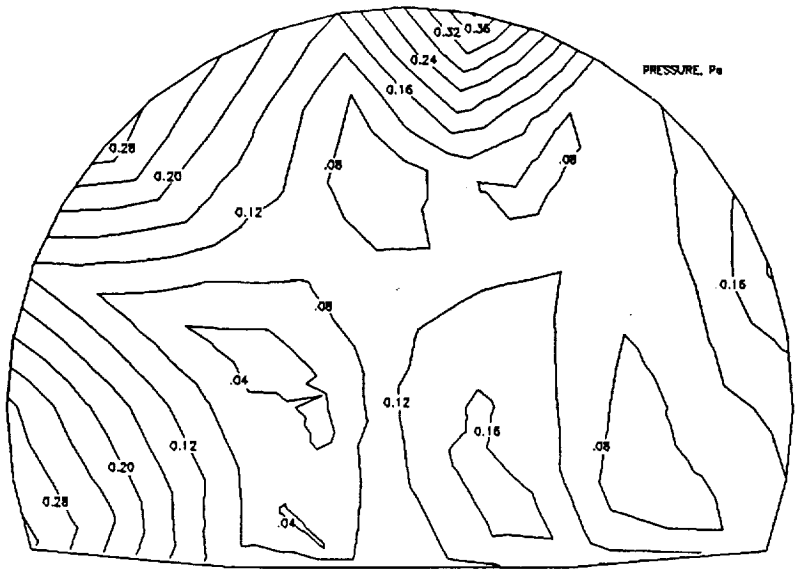

125 Hz

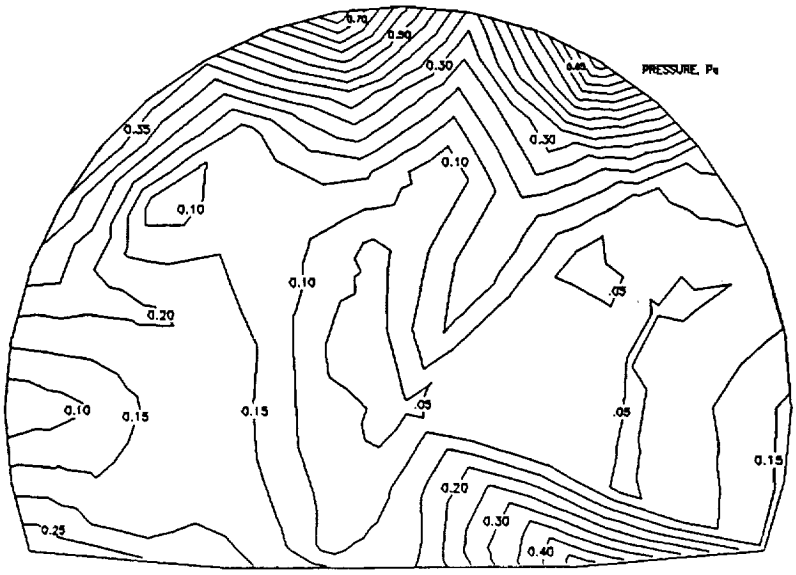

168 Hz

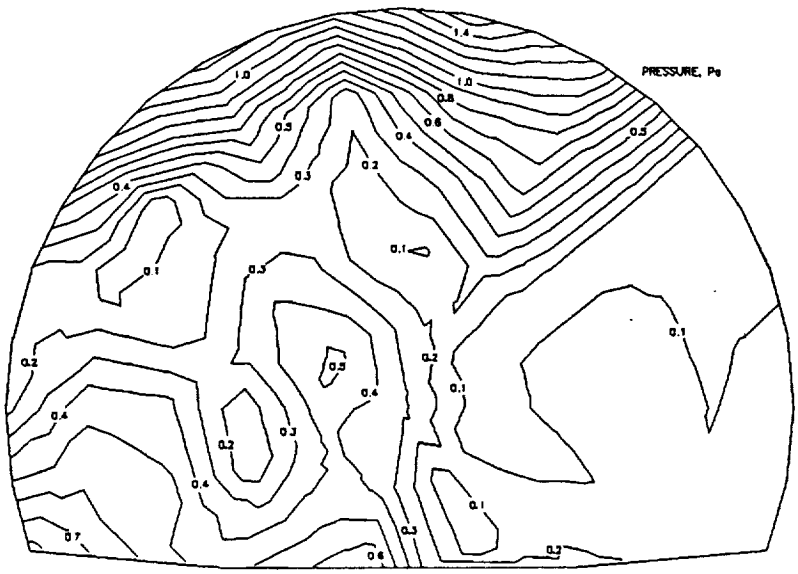

250 Hz

Figure 28. Cavity Pressure Distributions, Combined Single Speaker and Shaker Broadband Excitation

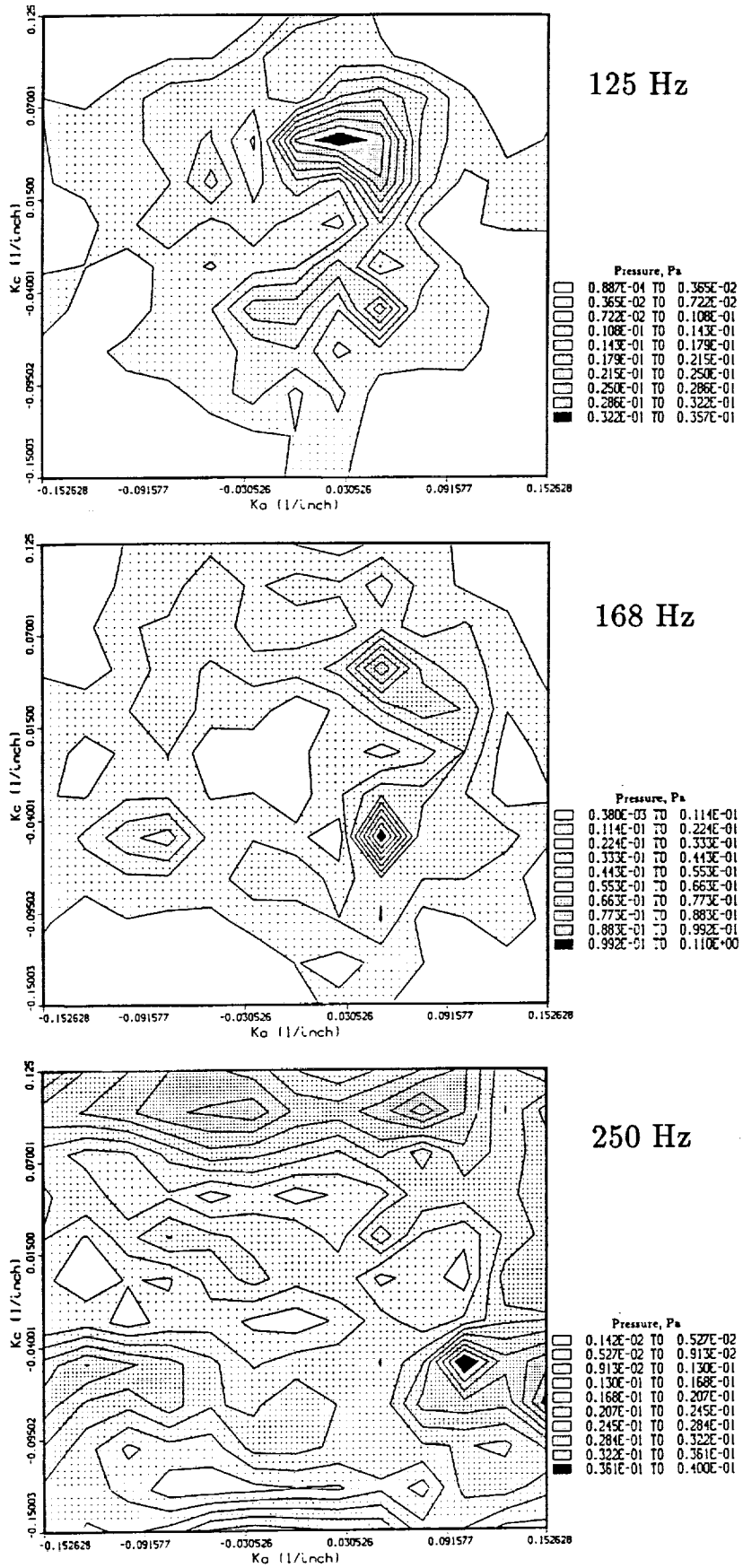

Figure 29. Pressure Wavenumber Maps, Combined Single Speaker and Shaker Broadband Excitation

6 Summary and Conclusions

A set of noise and vibration measurements were conducted in FARF to investigate the shell and cavity modal characteristics and the structural-acoustic coupling characteristics of the DC-9 aft fuselage test section, and the response of the fuselage to selected excitations. For these ground tests the fuselage configuration was similar to that of the Baseline Configuration used during UHB Demonstrator flight tests, with several noise and vibration control treatments installed but without trim panels or cabin furnishings.

The fuselage was exposed to six different excitations, including broadband acoustic excitation from a single interior and a single exterior loudspeaker, tonal acoustic excitation from a single exterior and multiple exterior loudspeakers, broadband vibration excitation from an exterior shaker, and combined broadband exterior acoustic and vibration excitation. For each excitation, noise levels were measured at 13 locations along the length of the cabin with an array of microphones throughout the cabin cross-section. For each excitation except that using the interior loudspeaker, vibration levels were measured on the fuselage surface with an array of accelerometers on the left side of the structure, and on two complete frame rings around the structure. Shaker input force levels were also measured, as well as exterior noise levels at selected locations.

Analyses of the transfer functions between the input source levels and the response noise and vibration levels were used to define the frequencies of the structural modes for frame 718, and the uncoupled and coupled transverse cavity modes at the same station. The structural and cavity mode shapes were then derived from the measured accelerometer and microphone data.

To study the structural-acoustic coupling, the first step was to make mode coupling predictions for a cylindrical shell and the FARF fuselage using the MDE method. Coupling of the structure and acoustic cavity is expected to occur at only those frequencies for which there is a structural mode and a cavity mode of identical mode order. The MDE predictions were used to identify candidate modes satisfying this condition, and thus guided the analysis of the measured data. To define the primary modes contributing to the fuselage vibration and cavity acoustic pressure at selected frequencies, a wavenumber analysis of the measured data was undertaken. The resulting wavenumber maps confirmed the MDE predictions that the N=2 structural mode would couple with the (n=2, p=0) circumferential cavity mode; from the measurements this was found to occur at 105 Hz. Further, the predictions and measurements both showed that there is no other major coupling of the structure and acoustic cavity.

Wavenumber analysis was also used to examine the response of the fuselage to the different types of excitation. This analysis showed that the fuselage response, in terms

of cabin noise levels, is dominated by low order modes (i.e., n=2) which appear to be independent of frequency for structural excitation. In contrast the response to acoustic excitation is dominated by modes whose order increases with frequency. The analysis also demonstrated that differences in response between broadband and tonal acoustic excitation were negligible, and differences in response between tonal acoustic excitation with and without wave-trace velocity effects were small. Finally, the fuselage response to combined acoustic and structural excitations was dominated by the response to the shaker; the wavenumber pressure was observed to be the sum of the separate wavenumber pressures from the individual acoustic and structural excitations.

The wavenumber analyses were found to be very useful in defining the structural-acoustic behavior of the fuselage. The wavenumber-frequency maps provide information about the structural-acoustic response of the fuselage/cavity that is usually not obtainable from conventional analyses based in the spatial domain.

7 References

[1] Simpson, M. A., et. al., "Interior Noise Control Ground Test Studies for Advanced Turboprop Aircraft Applications," NASA Contractor Report 181819, April 1989.

[2] Simpson, M. A., et. al., "UHB Demonstrator Interior Noise Control Flight Tests and Analysis," NASA Contractor Report 181897, October 1989.

[3] Fahy, F., *Sound and Structural Vibration: Radiation, Transmission and Response.* Academic Press Inc. (1985).

[4] Silcox, R. and H. Lester, "Propeller Modelling Effects on Interior Noise in Cylindrical Cavities with Application to Active Control," AIAA Paper 89-1123, Paper presented at the 12th Aeroacoustics Conference held at San Antonio, TX, April 10-12, 1989.

[5] Szechenyi, E., "Modal Densities and Radiation Efficiencies of Unstiffened Cylinders Using Statistical Methods," J. Sound Vib. 19, 1971, pp65-81.

[6] Williams, E. G., B. H. Houston and J. A. Bucaro,, "Experimental Investigation of the Wave Propagation on a Point Driven, Submerged Capped Cylinder using k-space Analysis," J. Acoust. Soc. Am. 87, 1990, pp513-522.

[7] Morse, P. M., *Vibration and Sound.* McGraw-Hill Company, New York (1948) (Reprinted by The Acoustical Society of America, 1981).

[8] Denke, P. H., "The MDE Method for Aircraft Cabin Interior Noise Prediction," ASME Paper 892372, Paper presented at the SAE Aerospace Technology Conference and Exposition held at Anaheim, CA, September 25-28, 1989.

NASA
National Aeronautics and Space Administration

Report Documentation Page

1. Report No.	2. Government Accession No.	3. Recipient's Catalog No.
NASA CR-187557		

4. Title and Subtitle
Fuselage Shell and Cavity Response Measurements on a DC-9 Test Section

5. Report Date
August 1991

6. Performing Organization Code

7. Author(s)
M.A. Simpson, G. P. Mathur, M. R. Cannon, B. N. Tran, and P. L. Burge

8. Performing Organization Report No.

10. Work Unit No.
535-03-11-03

9. Performing Organization Name and Address
Doouglas Aircraft Company
McDonnell Douglas Corporation
3855 Lakewood Blvd.
Long Beach, CA 90846

11. Contract or Grant No.
NAS1-18037

13. Type of Report and Period Covered
Contractor Report

12. Sponsoring Agency Name and Address
National Aeronautics and Space Administration
Langley Research Center
Hampson, VA 23665-5225

14. Sponsoring Agency Code

15. Supplementary Notes
Langley Technical Monitor: Kevin P. Shepherd
Final Report - Task 8, Subtask 1

16. Abstract

This report describes a series of fuselage shell and cavity response measurements conducted on a DC-9 aircraft test section. The objectives of these measurements were to define the shell and cavity modal characteristics of the fuselage, understand the structural-acoustic coupling characteristics of the fuselage, and measure the response of the fuselage to different types of acoustic and vibration excitation.

The fuselage was excited with several combinations of acoustic and mechanical sources using interior and exterior loudspeakers and shakers, and the response to these inputs was measured with arrays of microphones and accelerometers. The data were analyzed to generate spatial plots of the shell acceleration and cabin acoustic pressure field, and corresponding acceleration and pressure wavenumber maps. Analysis and interpretation of the spatial plots and wavenumber maps provided the required information on modal characteristics, structural-acoustic coupling, and fuselage response.

17. Key Words (Suggested by Author(s))	18. Distribution Statement
Acoustics Advanced Turboprop Aircraft Aircraft Noise Ground Tests Structural Response	Unclassified - Unlimited Subject Category - 71

19. Security Classif. (of this report)	20. Security Classif. (of this page)	21. No. of pages	22. Price
Unclassified	Unclassified	54	